Additively Manufactured Inconel 718: Microstructures and Mechanical Properties

Dunyong Deng

LiU LINKÖPING UNIVERSITY

Division of Engineering Materials
Departement of Management and Engineering (IEI)
Linköping University, SE-581 83 Linköping, Sweden

Linköping 2018

Cover image: A fracture surface of EBM IN718 after tensile test at room temperature.

During the course of research underlying this thesis, Dunyong Deng was enrolled in Agora Materiae, a multidiciplinary doctoral program at Linköping University, Sweden.

Abstract

Additive manufacturing (AM), also known as 3D printing, has gained significant interest in aerospace, energy, automotive and medical industries due to its capabilities of manufacturing components that are either prohibitively costly or impossible to manufacture by conventional processes. Among the various additive manufacturing processes for metallic components, electron beam melting (EBM) and selective laser melting (SLM) are two of the most widely used powder bed based processes, and have shown great potential for manufacturing high-end critical components, such as turbine blades and customized medical implants. The futures of the EBM and SLM are doubtlessly promising, but to fully realize their potentials there are still many challenges to overcome.

Inconel 718 (IN718) is a nickel-base superalloy and has impressive combination of good mechanical properties and low cost. Though IN718 is being mostly used as a turbine disk material now, the initial introduction of IN718 was to overcome the poor weldability of superalloys in 1960s, since sluggish precipitation of strengthening phases γ'/γ'' enables good resistance to strain-age cracking during welding or post weld heat treatment. Given the similarity between AM and welding processes, IN718 has been widely applied to the metallic AM field to facilitate the understandings of process-microstructure-property relationships.

The work presented in this licentiate thesis aims to better understand microstructures and mechanical properties EBM and SLM IN718, which have not been systematically investigated. Microstructures of EBM and SLM IN718 have been characterized with scanning electron microscopy (SEM), transmission electron microscopy (TEM) and correlated with the process conditions. Monotonic mechanical properties (e.g., Vickers microhardness and tensile properties) have also been measured and rationalized with regards to the microstructure evolutions before and after heat treatments.

For EBM IN718, the results show the microstructure is not homogeneous but dependant on the location in the components, and the anisotropic mechanical properties are probably attributed to alignment of porosities rather than texture.

Post heat treatment can slightly increase the mechanical strength compared to the as-manufactured condition but does not alter the anisotropy. SLM IN718 shows significantly different microstructure and mechanical properties to EBM IN718. The as-manufactured SLM IN718 has very fine dendritic microstructure and Laves phases in the interdendrites, and is "work-hardened" by the residual strains and dislocations present in the material. Mechanical properties are different between horizontally and vertically built samples, and heat treatment can minimize this difference. Results from this licentiate thesis provide the basis for the further research on the cyclic mechanical properties of EBM and SLM IN718, which would be the focus of following phase of the Ph.D. research.

Populärvetenskaplig sammanfattning

Additiv tillverkning (AM), även känt som 3D-printning, har väckt ett stort intresse inom flera olika sektorer så som flyg-, energi-, fordon- och medicinsk-industri på grund av dess möjlighet att tillverka komponenter som antingen är väldigt kostsamma eller omöjliga att tillverka med konventionella processer. Bland de olika additiva tillverkningsprocesserna för metallkomponenter är elektronstrålesmältning (EBM) och selektiv lasersmältning (SLM) två av de mest använda pulverbädds-baserade processerna och de har visat stor potential för tillverkning av avancerade kritiska komponenter, såsom turbinblad och anpassade medicinska implantat. Framtiden för EBM och SLM är utan tvekan mycket lovande, men för att fullt ut kunna realisera processernas möjligheter finns det fortfarande många utmaningar att övervinna.

Inconel 718 (IN718) är en nickelbaserad superlegering med en god kombination av bra mekaniska egenskaper och låg kostnad. Även om IN718 nu mestadels används som ett turbinskivmaterial, så var det huvudsakliga motivet för att utveckla IN718 att övervinna den låga svetsbarheten som fanns hos många superlegeringar på 1960-talet. Fördelen men IN718 är den långsamma utskiljningshastigheten hos förstärkningsfaserna γ'/γ'' vilket ger ett högt motstånd mot varmsprickor vid svetsning och vid den efterföljande värmebehandlingen. Med tanke på likheten mellan AM och svetsning så har IN718 tillämpats i relativt stor utsträckning för metalliska AM-processer och redan befintlig kunskap kan underlättat förståelsen för relationen mellan process-mikrostruktur-egenskaper även för AM.

Arbetet som presenteras i denna licentiatavhandling syftar till att bättre förstå mikrostrukturer och mekaniska egenskaper för EBM och SLM IN718, något som ännu inte är systematiskt undersökt. Mikrostrukturer för EBM och SLM IN718 har karakteriserats med svepelektronmikroskopi (SEM) och transmissionselektronmikroskopi (TEM) samt korrelerats till processbetingelserna. Statiska mekaniska egenskaper (t ex Vickers-mikrohårdhet och dragprovning) har också undersökts och kopplats till mikrostrukturutvecklingen före och efter olika värmebehandlingar.

För EBM IN718 visar resultaten att mikrostrukturen inte är homogen utan beroende på läge i komponenten. Dessutom är de anisotropa mekaniska egenskaperna troligen en konsekvens av porositeter uppradade och orienterade in en viss riktning snarare än kristallografisk textur. Eftervärmebehandling kan öka den mekaniska hållfastheten något jämfört med den direkt efter tillverkning, men detta ändrar inte anisotropin. SLM IN718 visar en signifikant skillnad i mikrostruktur och mekaniska egenskaper jämfört med EBM IN718. Direkt efter tillverkning har SLM IN718 en mycket fin dendritisk mikrostruktur med Laves-faser mellan dendriterna och kan betraktas som kallbearbetat på grund av den höga närvaro av restspänningar och dislokationer som finns i materialet. De mekaniska egenskaperna är olika mellan horisontellt och vertikalt byggda prover, och värmebehandling kan minimera denna skillnad. Resultat från denna licentiatavhandling utgör grunden för fortsatt forskning kring de cykliska mekaniska egenskaperna hos EBM och SLM IN718, vilket kommer att vara i fokus under den avslutande delen av detta doktorandprojekt.

Acknowledgements

First and foremost, I would like to acknowledge Chinese Scholarship Council (CSC) for the financial support, and Professor Ru Lin Peng for offering me this Ph.D. position, without which I would never have had the chance to present this work here.

Especially, I am indebted to my supervisor Professor Johan Moverare. You have provided me with every bit of advice, support, help and encouragement that guided me to move on. It is my greatest honour to have you as my supervisor, and I believe working with you will be the most valuable experience in my life.

Again, I would like to thank my co-supervisor Professor Ru Lin Peng. Thank you for sharing microstructural characterization skills and knowledge with me, and the fruitful discussions in the past years. Your diligence and devotion set a good example of a good researcher to me.

A collective acknowledgement goes to my colleagues at the Division of Engineering Materials, Linköping University. Thanks to the positive work atmosphere, the knowledge about research and life you shared with we, I have survived the dark and cold winters in Sweden. I am also grateful to all the administrators and technicians: Ingmari Hallkvist, Annethe Billenius, Rodger Romero Ramirez and Patrik Härnman, without you everything would have never gone so smoothly.

Further, I would like to express my gratitude to Professor Per-Olof Holtz for managing the Agora Materiae Graduate School, and to Professor Per Persson for teaching me how to operate TEM. To Hans Söderberg from Sandvik Machining Solutions, Håkan Brodin from Siemens Industrial Turbomachinery AB, Chamara Kumara and Paria Karimi Neghlani from University West, it is my pleasure to have collaborations with you and I am looking forward to further collaborations in the future. I am also highly obliged to Sandvik Machining Solutions, Sweden and Siemens AG, Germany for their generosities in providing samples for this work.

我自认为是一个不善表达的人，写这段致谢时总怕遗漏了谁，不敢轻易点名，也怕寥寥数语词不达意，但懂我的终将能在字里行间对号入座。求学在外多年，我最感谢我的父母亲和姐姐姐夫，你们替我承担了太多的艰辛，让我在本该养家糊

口的年纪依然能投身学术；俊沅、星翰和星豫，你们守护着我为人处世的一份童真。我要感谢我在林雪萍的小伙伴们，背井离乡的苦辣酸甜幸得有你们的分担，尤其感谢张丕敏，减肥大业一直没有荒废。有太多金属所的同学要感谢，即使我们天各一方，但你们依然愿意算好时差跟我讨论学术聊聊近况，或者只是毫无营养地互黑，这些情谊是我一辈子最宝贵的财富，不要太想我，但我很想大家。

<div align="right">

Dunyong Deng
邓敦勇
Linköping, January 2018

</div>

Contents

Part Part I:

Background & Theory

若廣學，懼其繁，但略說，能知源。
凡訓蒙，須講究，詳訓詁，明句讀。
《三字經》

CHAPTER 1

Introduction

1.1 Background

Additive Manufacturing (AM), also known as 3D printing, is a group of manufacturing processes that build components in an additive layer-by-layer or drop-by-drop fashion, which is able to obtain net shape components. Essentially, AM can offer great freedom to design and manufacture geometrically complex structures that are either impossible or considerably expensive by conventional processes, which rely on removing materials from monoliths. Given that, over the past decade, AM has attracted significant interest in manufacturing of critical metallic components with complex geometry in turbines and engines, as well as customised orthopaedic implants [1]. The development of the AM industry has shifted the focus from rapid plastic prototyping to metallic ready-for-use components. Unlike the plastic material, to additively manufacture metallic components, the interaction of the material and the melting source is relatively complicated and has not been well-understood. On the other hand, the high-end applications of metallic AM components are rather defect-intolerant, which require an optimization of the process to get desired microstructures and mechanical properties. The future of AM is doubtlessly promising, but to fully realize its potential, the process-microstructure-properties relationship needs to be but not yet systematically studied .

1.2 Research aims and questions

As one ot the nickel-base superalloys, Inconel 718 (IN718) was firstly designed and introduce to overcome the poor weldability of supealloys in 1960s. But now

3

IN718 is being used intensively in gas turbines and aero engines for discs and frames. Due to IN718's excellent weldability and similarity of the AM and welding precesses, IN718 has been widely applied in metallic AM fields to understand the fundamentals of AM processes. Electron beam melting (EBM) and Selective laser melting (SLM) are two of the most widely used AM processes for metallic components, and have very different processing conditions which would result in quite different microstructures and mechanical properties. The general aims of the present research are to characterize the microstructures and mechanical properties of IN718 manufactured by EBM and SLM, and the effects of heat treatments on microstructure evolutions and mechanical properties. In the present licentiate thesis, the main focus is placed on correlating the microstructures and monotonic mechanical properties (e.g., microhardness and tensile properties) with the processes and post heat treatments, based on which the cyclic mechanical tests would be performed in the future research. More specifically, this thesis addresses the following research questions:

For EBM IN718,

1. Is the as-manufactured microstructure homogeneous in EBM IN718?

   - Given the relatively high powder-bed temperature, the previously processed layers/parts inevitably experience longer "in-situ" annealing than the subsequently deposited layers/parts. Would this lead to the microstructural gradient?

   - Do the "contour" and "hatch" melting parameters applied to the frame and the core of a component, respectively, lead to different microstructures in the corresponding regions.

2. What are the mechanical properties of the as-manufactured EBM IN718?

3. What is the optimum heat treatment for EBM IN718?

For SLM IN718,

1. What is the as-manufactured microstructure in SLM IN718? Given the relatively low power-bed temperature and rapid cooling rate, would that cause segregation and residual stress in the as-manufactured SLM IN718?

2. Is the as-manufactured SLM 718 textured? How to rationalize the anisotropic mechanical properties with building orientations and textures?

3. How would the applied heat treatments affect the microstructure evolution and anisotropic mechanical properties?

1.3   Structure of the thesis

This licentiate thesis is divided into two parts:

1. Part I *Background* & *Theory*

2. Part II *Papers Included*

In Part I *Background & Theory*, the research project and the research questions aimed to address is first introduced to help the readers to get a picture of this licentiate thesis. Then, the more specific sections reviewing the Inconel 718, EBM, SLM, EBM and SLM IN718 are provided to give fundamental details on the investigating subjects. Following, the experimental methods are given as well as a summary of the papers included. The conclusions of the researches present in this thesis are also listed, based on which the future work is planed for the next phase of my Ph.D. research.

In Part II *Papers Included*, three journal papers that address the aforementioned research questions are presented.

CHAPTER 2

Inconel 718

Thanks to its good mechanical properties and low cost, Inconel 718 (IN718) is never out of the spotlight and has earned success in a wide range of applications, such as aircraft and land-based gas turbine engines, cryogenic tankage and liquid fuelled rockets. In this chapter, a review on IN718's history & use, chemical composition and phases, solidification metallurgy, post heat treatments, and anisotropy is provided. This review will surely offer insight into further discussion of additively manufactured IN718.

2.1   History and use

Inconel 718 is a nickel-base superalloy and was developed by International Nickel Company in 1959 [2]. The term "superalloy" refers to the high-temperature metallic materials which are employed in the extremely hot sections of the turbines, under the heavy and complex of loads but still display excellent resistance to mechanical and chemical degradation at temperatures close to their melting points [3].

IN718 has high strength, good weldability and fabricability. The unique combination of the aforementioned attributes has made IN718 itself a natural candidate material for many high temperature applications. The early major applications were on military engines in 1960s, for example the welded diffuser case for JT11 engine on the SR-71 Blackbird surveillance and reconnaissance aircraft [2]. Given its good mechanical properties up to 650 °C and competitive price due to its low cobalt and high iron content, IN718 has been increasingly applied in commercial engines from the late 1960's, specifically as the disc and rear frame material in gas turbines [2, 4]. Beyond these original and still major high temperature applications, IN718 is also being used as a generic alloy in nuclear, oil and gas industries

and cryogenic structures due to its excellent strength and aqueous corrosion resistance at ambient and low temperature [5, 6]. As a result, IN718 is the most widely used superalloy, accounting for 35 % of all superalloy production in the late 1980s [5], and over 50 % of the superalloy content in some engines [2].

2.2 Alloying elements in nickel-base superalloys

As its name implies, the principal element in nickel-base superalloys is Ni that forms the austenitic fcc matrix phase γ. And various amounts and combinations of alloying elements are also added to the γ matrix to achieve the desired microstructural features and mechanical properties. In broad terms, the common alloying elements that added in nickel-base superalloy are within certain ranges to obtain the optimal properties, and the addition ranges are listed in Table 2.1 [7].

Table 2.1. Compositional ranges of alloy elements addition in nickel-base superalloys

Element	Ni	Cr	Mo, W	Al	Ti	Co	Nb	Ta	Re
Range, wt.%	Bal.	5-25	0-12	0-6	0-6	0-20	0-5	0-12	0-6

- Bal. is the abbreviation of balance.

In general, each of these alloying elements is designed to partition to or form certain phases, providing the favourable properties. For instance, solid solution of Mo, Ta, W and Re in the γ matrix would impart the solid-solution strengthening; the addition of Al, Ti and Nb would tend to form strengthening precipitates γ' and γ'', from which the precipitate-strengthened nickel-base superalloys derive their strengths. The more specific roles of alloying elements in nickel-base superalloy is listed in Table 2.2 [7]. Note that these elements do not necessarily behave positively as listed, instead might form undesirable topologically close-packed (TCP) phases. The TCP phases might tie up strengthening elements in a non-useful form, and act as crack initiation sites due to their brittle nature [8].

Therefore, microstructures and properties of nickel-base superalloys are not simply correlated with the chemical composition, but more importantly interdependent of processing and alloying elements [7]. For each nickel-base superalloy, the whole processing, from melting to cast or wrought and to post heat treatments, must be tailored to make all alloying elements present in an appropriate form.

2.3 Phases and their properties in IN718

The composition ranges of alloying elements in IN718 are as shown in Table 2.3. Each alloying element servers certain purposes to obtain desired microstructure and properties, as shown in Table 2.2. Note that IN718 contains significant amount (about 20 wt.%) of Fe, due to which IN718 is occasionally classified as iron-nickel-base superalloy, and the manufacturing cost is considerably lowered.

Table 2.2. Alloying element effects in nickel-base superalloys

Element	Effects
Cr	Solid-solution strengthener, M_7C_3 and $M_{23}C_6$ carbides former, improve oxidation and hot corrosion resistance
Co	Solid-solution strengthener, raises solvus temperature of γ' $Ni_3(Al,Ti)$
Al	Strengthening phase γ' $Ni_3(Al,Ti)$ former, improve oxidation and hot corrosion resistance
Ti	Strengthening phase γ' $Ni_3(Al,Ti)$ former former
Nb	Strengthening phase γ'' Ni_3Nb former, MC and M_6C carbides former,
Fe	Solid-solution strengthener,
Mo	Solid-solution strengthener, MC, $M_{23}C_6$ and M_6C carbides former
W	Solid-solution strengthener, MC, $M_{23}C_6$ and M_6C carbides former
Ta	Solid-solution strengthener, MC carbide former, improve creep properties
Re	Solid-solution strengthener, retard γ' coarsening
C	M(C,N) carbonitrides former, grain-boundary strengthener
N	M(C,N) carbonitrides former
B	Grain-boundary strengthener, improve creep properties and rupture strength

Table 2.3. IN718 composition per Aerospace Material Specifications (AMS) 5383

Element	Ni (plus Co)	Cr	Fe	Nb (plus Ta)	Mo
wt.%	50.00 - 55.00	17.00 - 21.00	Bal.	4.75 - 5.50	2.80 - 3.30
Element	Ti	Al	Co	C	Mg
wt.%	0.65 - 1.15	0.20 - 0.80	1.00 max	0.08 max	0.35 max
Element	Si	P	S	B	Cu
wt.%	0.35 max	0.015 max	0.015 max	0.006 max	0.30 max

IN718 consists of the matrix phase γ and a variety of secondary phases. Since IN718 is a precipitate-strengthened superalloy, the presence and distribution of secondary phases in the matrix are the key to determining IN718's microstructure and properties. Table 2.4 summarized the crystal structures and chemical formulas of the commonly encountered phases in IN718.

Table 2.4. Phases commonly observed in IN718

Phase	Crystal structure	Chemical formula
γ	fcc	Ni
γ''	bct (ordered $D0_{22}$)	Ni$_3$Nb
γ'	fcc (ordered $L1_2$)	Ni$_3$(Al,Ti)
δ	orthorhombic (ordered $D0_a$)	Ni$_3$Nb
MC	cubic B_1	(Nb,Ti)C
Laves	hexagonal C_{14}	(Ni,Fe,Cr)$_2$(Nb,Mo,Ti)

2.3.1 γ' and γ''

In IN718 both γ' and γ'' are present and coherent with the γ matrix. Comparing the $D0_{22}$ crystal structure of γ'' to the $L1_2$ crystal structure of γ', the lattice parameter a of γ'' almost equals to that of γ', but the lattice parameter c is roughly doubled, by which γ'' is named. Both γ' and γ'' can strengthen the γ matrix by the following strengthening mechanisms [7]:

- The intrinsic strengths of γ' and γ'' phases.

- The lattice mismatch between the coherent γ'/γ and γ''/γ interfaces.

- Anti-phase boundary (APB) energy in the ordered γ' and γ'' phases, which is proportional to the energy required for dislocations to pass through these ordered phases.

When IN718 is nearly peak aged, the coherency strain hardening caused by the lattice mismatch confers principally strength to this superalloy [9, 10]. In IN718, γ' phase precipitates in a spherical morphology with a lattice mismatch of less than 0.5 % [11]. The presence of γ'' is in a disk morphology, and the tetragonal

lattice distortion ($c/a = 2.04$) results in considerable coherency strain [12]. The lattice mismatch between γ'' and γ matrix is reported as 2.86 % [10]. The relative volume fraction ratio of γ'' to γ' is about 3 [10, 13, 14], and Li et al. [14] suggested that heat treatment does not notably influence this fraction ration. The volume fraction of γ'' in peak aged IN718 is about 15 % while γ' accounts for just 4% [13, 15]. Therefore, though γ' phase does contribute to the strength of IN718, the principal strengthening is actually from γ'' phase due to both higher lattice mismatch and volume fraction.

2.3.2 δ

The γ'' phase in IN718 is metastable and can covert to the thermodynamically stable δ phase with a needle or plate-like morphology under thermal exposure. δ phase is incoherent with γ matrix, conferring rarely strength to the matrix when present in large quantities; on the contrary, the precipitation of δ phase would be at the expense of Nb, which associates with the loss of γ'' and therefore strength [7, 16]. The conversion from γ'' to δ is accelerated when the thermal exposure is over 650 °C, which limits the main applications of IN718 under 650 °C [17, 18]. The formation of δ is believed as a result of the excessive coherent mismatch between γ'' and γ matrix, and can be retarded by increasing the Al/Ti ratio and/or the Al + Ti content in IN718 [19]. With higher Al/Ti ratio and/or Al + Ti content, the size of γ'' is reduced as well as the lattice mismatch between the γ'' and γ matrix, therefore decreasing the driving force to form δ.

However, δ phase has favourable effects on the microstructure and mechanical properties under certain circumstances. Over 4% of δ phase at grain boundaries can efficiently inhibit the grain growth during heat treatment and working, which is an important aspect of current high-strength IN718 production [7, 20]. Globular grain boundary δ phase is beneficial to stress rupture [21, 22] and creep [21–23] properties, since the δ phase retards the intergranular crack propagation which is the predominant failure mechanism. The effects of grain boundary δ on fatigue properties are dependent on the fatigue fracture mode: having no influence on high cycle fatigue crack growth rate at 650 °C because of the transgranular fracture mode [23, 24], while improving the resistance to crack propagation along boundary under low cycle fatigue test where fracture is intergranular [25].

2.3.3 MC carbide

The predominant carbide phase in IN718 is Nb-rich MC phase, because the relatively high content of Nb promotes the formation of MC type carbide. Ti also incorporates in this MC carbide, resulting in its lattice parameter ranging between NbC and TiC phase but closer to the former [26]. Therefore, the primary MC carbide is denoted as NbC or (Nb,Ti)C in IN718. The primary MC carbide is mostly in discrete blocky shape and distributes in a non uniform manner within the grains as well as at the grain boundaries [26, 27].

- Intragranular MC carbide: The role of intragranular MC carbide in IN718 is less well documented. Generally, intragranular carbide can impede basic dis-

location movement but confer very small strength to the matrix, comparing the principal strengthening from γ'' precipitation. In addition, this carbide at a component's surface may be precracked or oxidized under thermal stresses, causing a unfavourable notch effect and degrading fatigue properties [7].

- Grain boundary MC carbide: MC carbides precipitated at grain boundaries promote the fracture mode transiting from transgranular to intergranular at room temperature [26]. During plastic deformation the stress would concentrate at the carbide and matrix interface, causing microcrack to relax the localized stress. When the MC carbides closely distribute along the grain boundaries, the microcracks would easily joint up and facilitate intergranular fracture. Though their effects on mechanical behaviour at elevated temperature have been rarely reported, it is expected that grain boundaries MC carbides discretely distributed and with appropriate size would restrict the grain boundary movement and give better rupture life.

As aforementioned, MC carbide being beneficial or detrimental to mechanical properties would depend on the size, distribution, precrack, oxidation and mechanical test condition. Mitchell et al. [28] concluded that TiN nitride can substantially promote the precipitation of MC carbide by acting as heterogeneous nucleation site, which would provide a potential of manipulating MC carbide distribution to optimize the mechanical properties.

2.3.4 Laves

Laves phase is a brittle intermetallic topologically close packed (TCP) phase, and is detrimental to mechanical properties. The formation of Laves phase is a result of Nb, Si and Mo segregation during solidification, where these alloying elements are rejected from the dendrites into the interdendrites [29, 30]. Chang et al. [31] suggested that the relatively high contents of Cr and Fe in IN718 are the necessary condition for Laves phase, aside from the segregation of Nb. The chemical composition of Laves might differ with solidification condition, but is generally referred as $(Ni,Fe,Cr)_2(Nb,Mo,Ti)$. In addition to its brittle nature, Laves depletes the matrix of Nb and the principal strengthening γ'' phase. Schirra et al. [32] summarized the effects of laves phase on the mechanical properties of wrought and cast+hot isostatic pressing (HIP) IN718 as following:

- Wrought: In wrought IN718 Laves phase precipitates as a continuous or semicontinuous network at grain boundaries. This results in significant reductions in tensile properties (ductility and strength) and toughness at room temperature, and ductility at elevated temperature. Further, the continuous Laves network acts as a preferred crack propagation site, accelerating fatigue crack propagation; while the semicontinuous network does not significantly affect the crack growth properties at elevated temperature.

- cast+HIP: Instead of forming the continuous or semicontinuous network, Laves phase presents as large irregular aggregate in cast+HIP IN718. Tensile properties at room temperature and stress rupture properties at elevated

temperature are significantly reduced. In addition, Laves also acts as a preferred crack initiation and propagation site, reducing the fatigue crack growth resistance and low cycle fatigue (LCF) capability.

In addition, though the IN718 is reputed for good wedablitiy in the context of its resistance to strain age cracking, the heat affected zone (HAZ) liquation cracking/microfissuring is still a major concern for IN718 during welding. During the heating cycles of welding, the low-melting-point Laves phase at grain boundaries can be liquated, forming grain boundary liquid. With the development of thermal stress during the cooling cycles of welding, the liquated grain boundaries are easily torn apart, leading to the hot cracks/miscrofissures [33, 34].

2.4 Solidification metallurgy

Due to the different partition behaviours of alloying elements, segregation of alloying elements during solidification is expected. Cast IN718 is regarded as heavily segregated: Fe, Cr, and Ni tend to stay in the dendrites, while Nb, Mo, and Si segregate in the interdendrites. This segregation can cause composition differences between the dendrites and interdendrites. For instance, the dendritic Nb content can be as low as 2 wt.%, while Nb level in the interdendritic regions can range as high as 12 wt.% [29]. Driven by the particular interest in Nb and the Laves and NbC features, a solidification diagram based on the Nb evolution was constructed under a cooling rate somewhat less than 500 °C/s by Knorovsky et al. [35], as shown in Fig. 2.1. The solidification begins with forming the primary γ dendrite, with Nb and C continuously enriching in the liquid. As γ growing, the Nb and C compositions in the liquid would satisfy the reaction L$\rightarrow\gamma$+NbC and form γ/NbC eutectic. This reaction consumes Nb and majority C in the remaining liquid, which shifts the remaining liquid composition back to the γ composition and forms γ again. As the γ growing, segregation of Nb in the remaining liquid would trigger another eutectic reaction L$\rightarrow\gamma$+Laves to terminate solidification, since the available C at this stage is not enough for L$\rightarrow\gamma$+NbC reaction. Antonsson et al. [36] compared the effects of cooling rate on IN718's solidification sequence, and suggested that:

- Irrespective of cooling rate, TiN can form before solidification of primary γ dendrites and provide nucleation sites for precipitation of NbC.

- At low and intermediate cooling rates (0.25 °C/s and 55.4 °C/s respectively), the solidification sequence is basically in good agreement with Knorovsky's solidification diagram, but there might be a reaction L+NbC$\rightarrow\gamma$+Laves at 1160 °C.

- At high cooling rate of 15000 °C/s, the solidification is terminated with L$\rightarrow\gamma$+NbC reaction.

Obviously, the cooling rate significantly affects the diffusions of alloying elements and therefore the formations and growths of phases. Tailoring the thermal

SOLIDIFICATION PATH
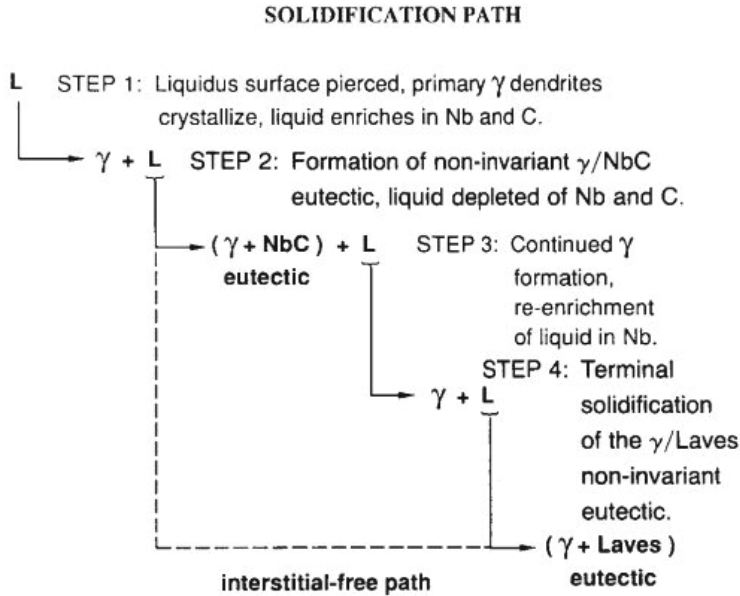
Figure 2.1. Non-equilibrium solidification path for IN718 [35]

conditions, rather than manipulation of chemical compositions, is essential to get the desired microstructure and properties [37, 38].

2.5 Heat treatments

Applying post heat treatments to IN718 is generally to remove the compositional segregation, and alter the presences and distributions of phases to obtain a homogeneous and appropriately strengthened microstructure. Specifically, homogenization is to dissolve the Laves phase, if there is any, and homogenize the compositional segregation; solution treatment is to homogenize the less-segregated microstructure and to precipitate small amount of δ; ageing is to precipitate the strengthening phases γ' and γ''. Note that the establishment of heat treatments is based on the microstructure inherited from the manufacturing process, the application as well as the desired properties.

2.5.1 Wrought IN718

IN718 is being predominantly used in the wrought form. Wrought is a process that mechanically works a cast billet or ingot several times at high temperature to get the final product. Therefore, wrought microstructure is generally more homogeneous and has finer grains than cast microstructure. The common heat

treatment details and applicable AMS specifications are summarized in Table 2.5. STD1 is the standard heat treatment for aerospace applications, gas turbine disks for instance, producing high rupture properties, room-temperature tensile strength and fatigue strength. For the tensile-limited applications, STD2 is preferred since it produces the best transverse ductility in heavy sections, impact strength and low-temperature notch tensile strength. Note that, all the grain boundary δ phases, pinning the grain boundaries and providing the notch ductility, would be dissolved by STD2, which would result in notch brittleness in stress rupture [7]. If a high-quality billet is used as the starting material and then forging is done below the δ solvus, direct ageing (DA) heat treatment is recommended for obtaining the highest tensile properties though a slight loss in stress-rupture capability [7].

Table 2.5. Heat treatments for wrought IN718

	Specifications	Solution heat treatment	Ageing heat treatment
STD1	AMS 5589 AMS 5596 AMS 5562 AMS 5662	927∼1010°C for 1∼2h, followed by rapid cooling, usually in water	719°C for 8h, furnace cool to 621°C, hold at 621°C for a total ageing time of 18h, followed by air cooling
STD2	AMS 5590 AMS 5597 AMS 5564 AMS 5663	1038∼1066°C for 1∼2h, followed by rapid cooling, usually in water	760°C for 10h, furnace cool to 649°C, hold at 649°C for a total ageing time of 20h, followed by air cooling
DA	-	-	719°C for 8h, furnace cool to 621°C, hold at 621 °C for a total ageing time of 18h, followed by air cooling

2.5.2 Cast IN718

Castings are intrinsically stronger than forgings at elevated temperature since the coarser grains in castings favour high temperature strength [7]. Though IN718 is being used in the wrought form as turbine disk material as mentioned, cast IN718 has still gained applications in aircraft engines for compressor and turbine frames, combustor cases, fuel nozzle rings and other hot engine structures [39]. Severe interdendritic segregation and presence of Laves phases, with/without cast porosity, make the cast microstructure considerably different from that of wrought form. Cast porosity can be closed by applying a HIP cycle; minimizing segregation can be achieved partly by the HIP cycle or by a separate homogenization heat treatment [5, 29, 39]. The homogenization temperature and duration are largely dependent on size of Laves phase: the bigger Laves phases, the higher homogenization temperature and longer homogenization duration [40]. Higher ho-

mogenization temperature can surely accelerate the homogenization proecess, but attention must be paid to incipient melting at grain boundaries caused by the rapid heating over the Laves solvus temperature [29]. Note that the grain boundary δ is dissolved during the homogenization treatment, which would cause unfavourable notch brittleness. Therefore, a solution treatment following the homogenization treatment is applied to re-precipitate δ phases. Ageing treatment for precipitating γ'/γ'' is basically the same as that for wrought IN718. Standard heat treatment for cast IN718 per AMS 5383 is listed in Table 2.6.

Table 2.6. Standard heat treatment for cast IN718 per AMS 5383

Homogenzation treatment	Solution treatment	Ageing treatment
1093±14°C for 1∼2h, followed by air cooling or faster cooling	954∼982°C for more than 1h, followed by air cooling or faster cooling	718°C for 8h, furnace cool to 621°C at 55°C/h , hold at 621°C for 8h, followed by air cooling

2.5.3 Powder metallurgy (P/M) IN718

Powder metallurgy (P/M) approach has been proposed to produce integral IN718 turbine rotors for space vehicles with short life but subjected to high temperature and high stresses [41]. The P/M route is able to produce finer grains, more uniform properties and near-net-shape components. By applying the STD1 heat treatment (see Table 2.5) to the P/M IN718 yields comparable tensile strengths to those of wrought IN718 but inferior ductility, which is attributed to the intergranular fracture induced by the decorations of brittle oxides (Al_2O_3, TiO_2) and MC type carbides at prior particle boundaries (PBBs) [41]. Further study showed that the oxygen pick up during the inert gas atomization of the master alloy would favour the formation of oxides and MC PPB network, drastically decreasing the ductility at elevated temperature and stress rupture properties [42]. The standard heat treatment per AMS5662 is not suitable for P/M IN718. Instead, a solution treatment at 1270 °C and a HIP at 1100 °C/130 MPa/3 h were suggested prior to the standard heat treatment per AMS5662 [43], in order to break the PPB networks.

2.5.4 Additively manufactured IN718

The microstructure of additively manufactured IN718 is largely dependent on the specific process history. With different process parameters, such as scanning strategy and component geometry, quite different as-manufactured IN718 microstructures can be obtained even under same manufacturing method, let alone different manufacturing methods. For the specific examples please refer to Chapter 5. Therefore, the heat treatment for AM IN718 should be customized with regards to its specific process history. Standard specification ASTM F3055 recommends a heat treatment for powder-bed-fusion additively manufactured IN718, please see Table 2.7. Note that this standard provides just a guideline for stress relief and

hot isostatic pressing treatments. Establishing the actual heat treatment should be as agreed between the component supplier and purchaser.

Table 2.7. Heat treatment recommended for powder-bed AM IN718 per ASTM F3055

Stress relief	Hot isostatic pressing	Solution + Ageing
1065±15°C for 85∼105min, performed while the components are attached to the build platform	1120∼1185°C at ⩾100 MPa inert atmosphere for 240±60min, followed by furnace cool to ⩽425°C	AMS 2774

2.6 Anisotropy

Single-crystal or columnar-grained nickel-base superalloy is widely recognized as elastically anisotropic, presenting different elastic properties when mechanical loadings are parallel to different crystallographic orientations [3]. As mentioned, IN718 is predominantly used in the polycrystalline wrought form, which is isotropic since the large number of randomly oriented grains average out the elastic differences. However, the additively manufactured IN718 is reported to be strongly textured with ⟨001⟩ crystallographic orientation parallel to the building direction. Elastic anisotropy of Ni (similar anisotropic behaviours are demonstrated nickel-based superalloys) is reviewed in general terms herein, providing the fundamental knowledge for anisotropic tensile properties discussed in the later chapters. For pure Ni, the ⟨001⟩ has the least elastic modulus 125 GPa, while the ⟨111⟩ has the highest elastic modulus 294 GPa, with the ⟨110⟩ between the two limits (220 GPa); for polycrystalline Ni, the elastic modulus is measured as 207 GPa at room temperature [3]. These anisotropic elastic properties strongly influence the low cycle fatigue performance: better fatigue properties is associated with the elastically soft directions, such as ⟨001⟩, than the elastically stiff directions, such as ⟨111⟩, because of both the greater elastic strain available to drive the fatigue process and higher yield stress along the elastically soft directions [3].

CHAPTER 3

Electron beam melting

Electron beam melting (EBM) is a powder bed based additive manufacturing process patented by Arcam AB founded in Sweden in 1997, and the first EBM production model S12 was launched in 2002 [44]. The schematic configuration of an Arcam EBM machine is shown in Fig. 3.1a. Until now Arcam AB is still the only pattern holder for EBM processes and hardware, and powder supplies for EBM processes are also available from Arcam AB's own manufacturing company. Research activities on self-built electron beam melting machines based on the similar principles can also be found in literatures, but gave inferior performances to the Arcam AB's hardware [45]. In this chapter, the EBM process is reviewed but not just limited to that conducted with Arcam AB's hardware, to provide readers a broad view of the nature and applications of this process.

3.1 Introduction

EBM is a powder-bed fusion (PBF) process that uses electron beam to selectively melt the defined geometries at each layer and simultaneously fuses with previously solidified layers in a powder bed, by which method a 3D part is built. The use of an electron beam as the energy source offers specific advantages to this process. To enable the electron beam to work appropriately, high vacuum is maintained throughout the process, making EBM particularly suitable for manufacturing the chemical-sensitive materials, e.g., titanium. With the electromagnetic lenses, the electron beam can be focused or defocused to adjust the energy density for heating or melting purposes. In addition, the state-of-the-art deflection electronics enables the extremely rapid movement of electron beam within the building area, allowing melting at multiple points simultaneously and achieving high melting capacity and high productivity[46]. Further, it is worth mentioning that with the rapid

movement and defocus of the electron beam, the entire powder bed is heated and maintained at an relatively high building temperature throughout the process, producing the components free from residual stresses. On the other hand, the nature of electron beam limits this process to conductive materials, since only conductive materials can be heated by absorption of the energy carried by accelerated electrons. In addition, inappropriate electrostatic charges in powders might lead to an undesirable smoke phenomenon, which would suddenly cause the uncontrolled repulsion/blowing of the powders and even process instabilities/termination [47, 48]. The detailed process will be given in the following sections.

3.2   Process

Fig. 3.1b illustrates the typical building cycle of an EBM process. A base plate is first preheated slightly above the building temperature, before applying the first layer of powder. As shown in Fig. 3.1b, for each building cycle, the base plate is lowered and a new layer with a identical thickness of powder is laid on the top, then the electron beam scans over this powder layer to consolidate the powders in a predefined pattern. Note that the scanning of electron beam is firstly to preheat and slightly sinter the current powder layer, then melt the current powder layer and form a solid layer of the build. This cycle would be repeated until the build is finished. After the building process is finished, the whole powder bed starts cooling down itself. Accelerated the cooling is optional by injecting appropriate amount of helium into the chamber.
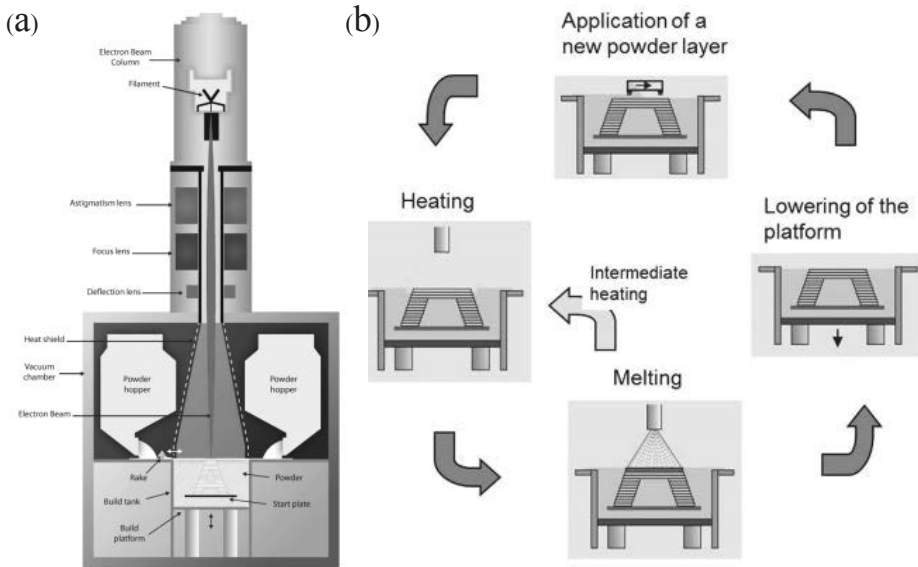
Figure 3.1. (a) Schematic configuration of an Arcam EBM machine [49], (b) schematic building cycle of an EBM process [45].

3.2.1 Applying powder layer

Powder layer is applied by raking the powders supplied from the powder hopper, as shown in Fig. 3.1a. Before raking the powders, the build platform is lowered to certain distance to provide space for a new powder layer, and this distance is the powder layer thickness. The powder properties, i.e. size, shape, morphology, composition, porosity and flowability, significantly affect the process stability and resulted material properties [45]. While finer size of the powder might give better geometry accuracy and surface roughness, it is also easier for finer powders to trigger the unfavourable smoke phenomenon than coarser powder. To compromise, the powder is recommended to have a particle size between 45 and 100 μm according to Arcam's specification [50] with a bimodal size distribution [51] and smaller fraction of 25~45 μm powder [52]. The perfect spherical morphology without small satellites attached is favoured since it can result in higher flowability, which is important for raking an uniform powder layer. The powder morphology largely depends on the powder manufacturing process: gas atomization (GA) powders are generally in spherical shape but are mostly attached with small satellite particles, rotary atomization (RA) powders are basically semi-spherical, while plasma rotating electrode process (PREP) powders are almost perfect round without satellites [53]. In addition, gas induced porosity is common in GA and RA powders, while PREP powder is noted as absent from such porosity [53–55]. For the aforementioned reasons, PREP powders are preferred.

3.2.2 Preheating

A preheating step, during which the electron beam is defocused and scans over the powder layer several times, is performed before this powder layer is actually melt and fused together. This is to slightly sinter the powders for better electric conductivity and process stability, and to maintain the relatively high building temperature within the whole building chamber [45].

Sintering is a solid state process that atoms at the particle interfaces diffuse to the contiguous particles and form a "neck", binding them together at the temperature between half melting point and full melting point [56]. As a result of this slightly sintering, the electric conductivity is improved compared to the loosely stacked state, and the smoke phenomenon is therefore efficiently prevented [57]. A partial pressure of helium (4×10^{-3}mbar) is also introduced into the vacuum chamber to prevent smoke [46, 58]. When the entire process is finished, the build will be embedded within a slightly sintered powder bed. The sintered powders can be easily removed by sand blasting, and with appropriate sieving these powders can be nearly completley recycled [45].

As mentioned, to slightly sinter the powder bed, the preheating temperature have to be over half melting point. Therefore, the powder bed is maintained at relatively high temperature throughout the process. For instance, for Ti6Al4V it is typically between 550 to 700 °C [58–60], and for IN718 it can be over 900 °C [61, 62]. This leads to mostly full in-situ stress relief and no residual stress in the as-manufactured microstructure [63].

3.2.3 Melting

Melting is, after the preheating stage, to fully melt the powders and fuse them together to form a solid component as designed. During the melting stage, two scanning strategies, namely contour and hatch, are typically applied: contour is to "draw" the frame of the build, while hatch is to "fill in" the interiors of the build. Contour strategy uses the *MultiBeam* technology that splits the electron beam into multiple spots and rapidly "draw" the frame, enabling optimization of surface finish, precision and build speed simultaneously [46, 64]. Differently, hatch strategy scans continuously the beam in a forwards-and-backwards pattern at each layer, and the scanning direction is rotated by certain angel between each layer. The process parameters, such as beam power, beam focus offset, beam velocity, line offset (the distance between two adjacent scanning passes), are different with these two scanning strategies, resulting in considerably different thermal conditions [65] and therefore microstructures [66, 67].

3.3 Defects

As mentioned, the powder bed of the EBM process is maintained at relatively high temperature, which leads to every low residual stresses in the as-manufactured microstructures. Therefore, unlike the selective laser melting (SLM) process where residual stress is the major concern for causing distortion and delamination, the common defects in as-manufactured EBM components are porosity and surface roughness.

3.3.1 Porosity

Typical porosities found in EBM builds are shown in Fig. 3.2. Porosity can be catalogued as process-induced (Fig. 3.2a and b) and powder-induced (Fig. 3.2c and d).

The process-induced porosity, referred as *lack of fusion*, is formed due to the unoptimized process parameters, specifically inappropriate energy input [61]. This kind of porosity is mostly irregular in shape and size varies from micrometer to millimetre.

- Insufficient energy input would lead to a region of powder that cannot be fully melt and fused together. Un-melt powder is usually visible in or near this kind of porosity, as shown in Fig. 3.2a and b.

- Too much energy input would lead to spatter ejection, where a region of powder is though fully melt but the melt is spattered away. As a result, lack of melt to bond the desired melt region.

Even with optimized process parameters, impurities or gas-trapped voids in the virgin or recycled powder can directly form the powder-induced porosity. The pores induced from impurities are with impurities debris inside, and the size is within the range of powder size, as seen in Fig. 3.2c. The trapped gas within the
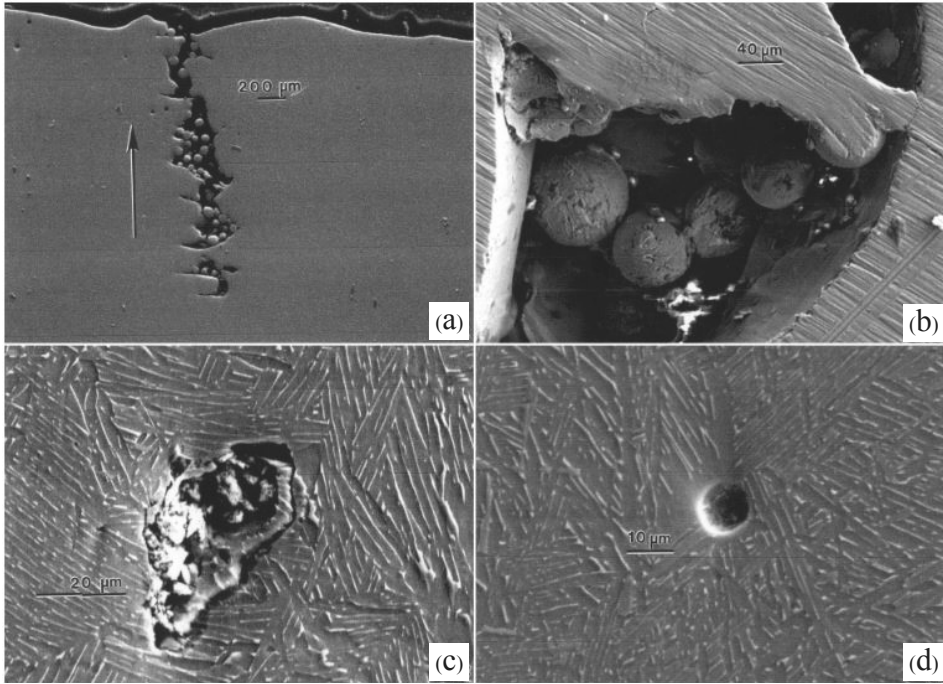
Figure 3.2. Examples of porosity defects in EBM Ti6Al4V builds: (a) continuous beam tripping resulting in unconsolidated region progressing with build (arrow); (b) unmelted pocket; (c) build flaw revealed in grinding and polishing sample; (d) hemispherical (spherical) gas void [68].

gas atomized powders, despite the high vacuum atmosphere in the EBM chamber, cannot necessarily escape from the melt but embed in the resulted microstructure due to the rapid solidification process [66, 69], as seen in Fig. 3.2d.

The presence of porosities is detrimental to the mechanical properties, especially for the crack initiation and propagation resistances. Therefore, either tuning the process parameters or improving powder the feedstock quality can reduce the porosities during the process. On the other hand, HIP is widely applied to the as-manufactured materials to improve density. HIP can significantly reduce the porosities, but still cannot result in 100% dense microstructure [70]. HIP reduces/eliminates the process-induced porosities [71], but might not close those gas-trapped pores since the trapped gas can still "prop up" the pores [72].

3.3.2 Surface roughness

As-manufactured EBM components' surfaces are generally rougher than those manufactured with SLM, due to the sintering occurred at componenets' surfaces. The roughness is largely affected by the process parameters: it increases with increasing the beam current and decreasing scan speed and focus offset [73]. Körner

et al. [45] suggested that the coarser powder, thicker powder layer and larger beam size lead to higher EBM surface roughness than that of SLM. Though post surface machining is able to improve the surface condition for simple-geometry builds, it offers no solutions for complex-geometry components.

3.4   Materials manufactured with EBM

Various materials have been manufactured with EBM to investigate their microstructures and mechanical properties, and to explore the possibilities for high-end applications. The most reported materials are listed as following:

- **Ti-6Al-4V**: The vacuum atmosphere in the EBM chamber ensures a clean environment and avoids the contaminations from gases during processing, which is therefore suitable for EBM titanium alloys, in particular Ti-6Al-4V [48, 51, 52, 58, 60, 69, 73]. In addition, since Ti-6Al-4V has superior properties for numerous potential applications, it is the most widely researched material for EBM process.

- **Nickel-base superalloys**: Nickel-base superalloys also attract considerable interest in the field of EBM due to their excellent mechanical performance for high temperature applications and the difficulties for machining complex-geometry components. Currently, the major EBM Ni-base superalloy research is focus on IN718 [53, 74–78] and IN625 [79, 80] because of their weldabilities. However, the relatively high chamber temperature during process enables the possibility of manufacturing those γ' strengthened Ni-based superalloy. For instance, Rene 142 [81] and CMSX-4 [82], which are recognized as less-weldable, have been successfully manufactured with EBM.

- **CoCr**: CoCr alloy is widely used within orthopaedic field, mostly load-bearing orthopaedic prostheses, due to its high strength, wear-resistant and excellent bio-compatibility [83]. However, due to the high stiffness of CoCr, stress shielding and bone resorption have been a concern. Constructing a open cellular structure has been proved to lower the stiffness of CoCr and provide better match with the human bones [84, 85]. Customized open cellular CoCr strctures have been successfully manufactured with EBM for load-bearing applications with comparable biological response of Ti6Al4V [86].

3.5   Future work

Though the preliminary researches on EBM have shown great potential, the process itself is still far from being completely developed [45]. Further work on the following aspects might bring about some breakthroughs:

- *Optimization of process parameters*: So far the factually full dense has not yet achieved in the as-manufactured EBM components. The presence of

porosities is intolerable for critical components, since it might significantly impair the mechanical properties. In addition, there are still opportunities for further enhancements for the as-manufactured surface roughness, which can be a major concern for fatigue properties. So, optimizing the process parameters is practical to overcome these shortcomings.

- *Fundamentals of EBM process*: To protect from the radiation from electrons, a leaded-glass is mounted on the viewport of the EBM machines, due to which the exact process and the thermal profile cannot be well-monitored[87]. Besides, the instantaneous interaction of the moving beam and powders is rather complicated and is not consistent through the whole build. Mathematical-physical finite-element (FE) model is a good way to understand the fundamentals of EBM process, which should involve (a) modelling of materials properties, (b) modelling of thermal conditions and (c) implementation of the aforementioned aspects [88]. Currently, the reported models are simplified and cannot correlate well with the EBM process. Therefore, comprehensive models are needed to get better understanding of EBM process, which in return can guide the optimization of process parameters.

- *Microstructure engineering*: The microstructure produced by EBM is highly dependent on the building thermal history. One example is a microstructural gradient along the building direction observed in as-manufactured EBM IN718 (please refer to the included Paper II). Such a unique feature might indicate the potential of engineering the microstructure to obtain desired gradient properties with EBM process.
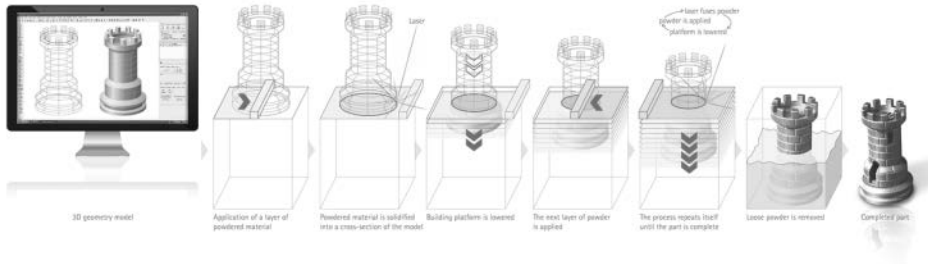
Selective laser melting

When it comes to laser-base powder-bed fusion (PBF) additive manufacturing, one might encounter so much confusion about the nomenclature of different technologies or processes under this category: Selective Laser Sintering (SLS), Direct Metal Laser Sintering (DMLS), Selective Laser Melting (SLM) and so on. Then one might ask what the differences are between these technologies. "It depends on who you ask. Some people use the terms interchageably, others maintain that there are sharp differences between them and others think that it is just a bunch of Germans who used to all be friends playing word games in English. [89]" as Joris Peels wisely explained the situation. In this chapter, a brief introduction would be provided to the aforementioned different technologies, and then the general review of this laser-base melting process would be given, to help the readers gain an overview of the whole category.

4.1 Introduction

First of all, Selective Laser Sintering (SLS), Direct Metal Laser Sintering (DMLS) and Selective Laser Melting (SLM) follow essentially the same process philosophy and procedure, as shown in Fig. 4.1. After the component's 3D model has been processed and transferred to the laser-base AM machine, the building process starts with applying a thin layer of powder on the building base plate. A laser beam is then used to melt the powders at the locations defined by design data for the current layer, followed by lowering the base plate and applying a new layer of powder with the identical thickness on the top. Once again, the laser beam melts the powders at the predefined locations and fuses them with the previous layers. This cycle is repeated until the component is finished as designed, after which the component is removed from the loose powder bed.

Figure 4.1. General process procedure of laser-base powder-bed fusion (PBF) additive manufacturing technologies. [90]

If to distinguish these four technologies in a literal way:

- Selective Laser Sintering (SLS) is a general term of essential sintering process rather than a fully melting process. SLS can be applied to a variety of materials, i.e. plastics, polymers and metals. The powders applied in SLS can be multiple-component (typically one component that has low-melting point is melt and binds powders together) or single-component (is partially melt and binds the unmelt parts together) [56].

- Direct Metal Laser Sintering (DMLS) is a SLS-derived technology and is specifically applied to metallic materials. At the early phrase of DMLS, this process was applied to fuse powder mixture, but did merely partially melt the low melting point phase, remaining the high melting point phase unmolten and significantly amount of porosities [56, 91]. However, with the optimization of laser parameters, the full melting can be achieved during this "sintering" process [92–94]. Nowadays, the DMLS process is applied to actually fully melt the powders rather than just "sinter" the powders, though it is called as "sintering". As noted in ISO/ASTM 52900:2015 standard, the word "sintering" is a historical term and a misnomer, as the process typically involves full or partial melting, as oppsed to traditional powdered metal sintering [95].

- Selective Laser Melting (SLM) is straightforward a fully melting process as the name suggests. Currently, the selective laser melting process has been widely applied to additively manufacturing metallic components. Different vendors have commercialized their additive manufacturing systems essentially based on the selective laser melting process. Due to the patent and trademark related issues, nomenclatures of these additive manufacturing systems are differently. For instance, Direct Metal Laser Sintering (DMLS) is for EOS, Selective Laser Melting (SLM) is for SLM Solutions, LaserCUSING is for Concept Laser, RenAM is for Renishaw, Direct Metal Printer (DMP) is for 3D Systems and TruPrint for TRUMPF. However, the differences in

these nomenclatures don't really reflect the differences in their abilities and applications.

Part of this Ph.D. research is to investigate the microstructures and mechanical properties of IN718 manufactured by selective laser melting process, as mentioned in Chapter 1. Though the manufacturing was technically a DMLS process performed with a EOS machine, this IN718 sample is still named as SLM IN718 to avoid the unnecessary confusion. Hereby, the discussion about selective laser melting process would not be specifically referred to a manufacturer or manufacturing system, and the acronym SLM would be used.

4.2   Process

The typical process cycle for SLM is as illustrated in Fig. 4.1. If compared with the EBM process cycle, one can find that there is not a top down laser-beam preheating stage before melting the powder. That can be attributed to the relatively low power and small laser beam size, which can not efficiently preheat the whole powder bed and maintain it at a elevated temperature. Thus, to preheat the base plate, a resistive heat module is commonly installed underneath the building platform [96]; to preheat the powder bed before melting stage, an extra laser source is optional with certain systems [97].

Another thing worth to note is that during the melting stage, contour and hatch scanning parameters are normally applied to draw the "skin" and fill in the interior volume, respectively, as that in EBM process. Differently, contour followed or following by hatch can vary from research to research [98, 99]. And the contour is generally associated with lower power and lower scanning speed to improve the geometry accuracy and roughness, while the hatch is adjusted to higher power and higher scanning speed to increase the productivity [98, 100].

After the building process is finished, the component is embedded within a loosely aggregated powder bed and it can be easily removed from the powder bed. However, stress relief treatment, if required, is typically performed before removing the component from the base plate.

4.3   Defects

The common defects associated with SLM components are residual stress, crack and porosity, among which residual stress can be a major concern for both manufacturing process stability and geometry accuracy (e.g., distortion). Though the surface roughness of the as-manufactured SLM components is still slightly higher than that of the conventionally machined surfaces, it is superior to that manufactured via EBM due to smaller laser beam and powder size. Thus, surface roughness is not discussed in this section.

4.3.1   Residual stress

The root cause for residual stress in SLM process is the non-uniform temperature gradient localized in the heated zone during melting, which would result in a complicated non-uniform deformation during the rapid cooling when the laser beam moves away. Residual stress, depending on the magnitude with respect to the material's strength, might significantly influence the components' dimensional and geometry accuracy as well as mechanical properties. Even worse, it might lead to crack formation, delaminating the components or disconnecting the components from the building platforms, which would terminate the ongoing manufacture process [101].

Different approaches have applied to profile the residual stress distribution during SLM process or in the as-manufactured components. Simplified mechanism and model have been proposed to explain the introduction of residual stress during the SLM process, and suggested tensile stress in the upper portion of heated zone or layer while compressive stress in the lower portion of heated zone or layer [102]. To more accurately predict the residual stress development, finite element analysis coupling thermal aspects and powder/mechanical properties are preferred [101, 103–105]. Experimental measurements using X-ray [105–107] or neutron diffractometer [101, 108] have been reported, but the results are unable to present the residual stress profile within the whole component, since these measurements were performed on sporadic spots on the superficial region. Note that the residual stress might be relaxed and re-distributed if the component is directly removed from the base plate after the process, and experimental measurement on this kind of sample would probably give artificial results. And if to summarize the results from the aforementioned references, no common conclusion on the residual stress profile can be reached, but the development of residual stress is shown as largely dependant on process parameters; and the residual stress is mostly as high as or even higher than the yield strength of the building material.

Optimizing the process parameters is a practical way to minimize the residual stress accumulated during process. Preheating the powder bed can reduce the thermal gradient and cooling rate in SLM process and therefore efficiently reduce the residual stress accumulated in the components [96, 109–111]. Optimized scanning strategy (i.e., alternating scan direction [99, 101], shorter scan length [112], lower scanning speed [112] and re-scanning [109]) can also significantly minimize the residual stress. Specifically, the "island" scanning strategy (i.e., each layer is divided into small islands, within each island the scan vector is alternately forward-and-backward, the vectors in the neighbouring islands are perpendicular to each other, and in the subsequent layer the island pattern is shifted slightly) has shown to effectively decrease the overall residual stress during process [108, 113, 114].

4.3.2   Crack

Crack is mostly attributed to the relatively high and localized residual stress, as mentioned above. By forming and/or expanding the cracks, the residual stresses is released. On the other hand, Song et al. [115] suggested that the serious segregation of Nb and Mo at grain boundaries would increase the tendency of

forming low melting point eutectic phase, and incipient melting might happen under the complicated thermal condition and form cracks at the grain boundaries.

4.3.3 Porosity

Two types of pores, namely spherical and irregular, are mostly found in as-manufactured SLM components. The spherical pores are attributed to: (a) the inert gas is involved into the melt pool and (b) the gas trapped inside the powder can not escape from the melt pool [72, 115]. These spherical pores are less deleterious to the components' mechanical properties, while the irregular pores, which can raise the concentration of stress under service and lead to failure, are the major concern for controlling the porosities. Thijs et al. [116] suggested that the large pores with the dimensions of $100{\sim}200$ μm result mostly from (a) the accumulations of the powder denudation within the melt pools within a layer, and (b) the surface roughness across the layers. The balling phenomenon (i.e., the melt pool is solidified into discontinuous balls due to poor wettability) can also introduce a large number of irregular pores enclosing non-molten powder and worse surface roughness [117–119].

4.4 Materials manufactured with SLM

Compared to EBM, the materials that are applicable to SLM are not just limited to the conductive ones. Instead, ceramics and composites components can also be manufactured via SLM, though it is more challenging than to manufacture the metallic parts. The most common metallic materials worked with SLM are iron-base alloys, titanium alloys, Al-Si alloys and nickel-base superalloys.

- **Iron-base alloys**: Iron-base alloys are one of the metallic materials widely applied to SLM at its early phase. The purpose at that early phase was mainly to understanding the SLM process [120–122], and with the development of SLM process the focuses and aims gradually shift to exploring the possibilities of manufacturing high-value added components. The most commonly reported SLM iron-base alloys include 316L stainless steel [123–128]. Other steels, e.g., M2 tool steel [96, 129–131] and 17-4 PH stainless steel [132–136] have also been reported.

- **Titanium alloys**: Titanium alloy, specifically Ti-6Al-4V [72, 137–143], is the most investigated material for SLM process. Manufacturing titanium alloys via conventional methods is relatively difficult, since Ti is highly reactive and sensitive to chemical impurities, such as O, N and H. With this regard, SLM is superior to conventional manufacturing methods since the inert gas in the SLM chamber can provide a protective atmosphere. On the other hand, manufacturing titanium alloys via SLM is largely driven by the applications of customized medical implants and topological-optimized aircraft components. The initiatives of manufacturing Ti-6Al-4V components via SLM are almost the same to that of EBM process. However, due to different thermal

profiles in these two processes, the typical as-manufactured SLM Ti-6Al-4V microstructure is acicular α' in contrast to the acicular $\alpha+\beta$ in EBM Ti-6Al-4V microstructure. With post heat treatments, the SLM Ti-6Al-4V might be modified to lamellar $\alpha+\beta$ or lamellar $\alpha+\beta$ + globular α, while EBM Ti-6Al-4V still retains the same acicular $\alpha+\beta$ phases [144], giving comparable mechanical properties. Commercially pure titanium (CP-Ti)[145–148] and Ti-6Al-7Nb [149, 150] which have better mechanical properties and biocompatibility than Ti-6Al-4V have also been manufactured via SLM for medical implants applications.

- **Al-Si alloys**: Due to their attractive combination of low weight, high heat conductivity and mechanical properties, Al-Si alloys (AlSi10Mg [151–157] and Al-12Si [158, 159]) have wide applications in aerospace, automotive industries as heat exchangers. AlSi10Mg and Al-12Si are hypoeutectic alloys whose mechanical properties are largely dependant on the morphology of eutectic silicon. By adding small amount of Mg, Mg_2Si can form and considerably strengthen the matrix without compromising the other mechanical properties. Manufacturing Al-Si components via SLM is driven by: (a) the relatively rapid solidification rate associated with SLM process, which can lead to finer microstructures and more homogeneous distribution of eutectic silicon to improve the mechanical properties and (b) components' geometry design freedom. However, compared to other SLM materials, manufacturing Al-Si alloys faces different challenges, such as poor flowablitiy of powders, high reflectivity along with high thermal conductivity and porosities.

- **Nickel-base superalloys**: Nickel-base superalloys are the natural candidates for additive manufacturing including both SLM and EBM processes, due to the difficulties and limitations of conventional manufacturing methods, e.g., segregation, poor workability, machining cost. As that for titanium alloys, employing SLM or EBM to manufacture Ni-base superalloys would depend on the specific case or application, since each process has its pros and cons. So far, the Ni-base superalloys applied to SLM are mainly the weldable ones, i.e., IN718 [113, 160–167], IN625 [79, 80, 168, 169], Hastelloy X [170–174], Nimonic 263 [110], which have low additions of both Ti and Al and are less susceptible to strain age cracking. Expansion to the less-weldable Ni-base superalloys has also been attempted, such as IN939 [175], IN100 [176], IN738LC [177–181], CM247LC [114, 182–184] and Rene 142 [81]. These researches have shown the great potential for manufacturing complex-geometry critical and functional components for high temperature application via SLM.

4.5 Future work

As that of EBM, the preliminary researches on SLM have demonstrated the great potentials of this process. Nevertheless, there are still many technical challenges to overcome before this process can be fully taken advantage of.

- *Understanding the solidification metallurgy*: The physical phenomena during the extremely short interaction of laser and powder is rather complicated, which results in quite different solidification behaviours to that of conventional manufacturing methods. Understanding this physical phenomena is vital to understand the SLM process and in turn guides the optimization of the process. The rapid cooling rate, on one hand is beneficial to homogeneous and fine microstructure, but on the other hand hinders the full understanding of solidification metallurgy. Correlating the dendrite arm spacing with cooling rate is commonly applied to analyse the solidification behaviours in, for instance, cast and welded materials. However, such correlation by extrapolation might give poor accuracy for the SLM cases [184]. Therefore, the future work on the solidification metallurgy might have to be thought outside the box of traditional solidification scope.

- *Material development*: As mentioned, the intrinsic weldability of a material, to some degree, determines its applicability to the SLM process. To put it in another way, SLM cannot be applied to those alloys, which suffer considerably from thermally induced cracks during the process, just by optimizing process parameters [174]. But instead, by optimizing the alloying element additions within the specification range, it has been demonstrated that the material's crack susceptibility can be reduced without compromising its mechanical properties [174, 185]. Therefore, developing materials that are specifically for SLM process allows the wider applications of SLM.

- *Process parameter optimization*: So far, the researches on SLM mostly deals with the process parameters (e.g., laser power, scanning strategy, scanning speed, powder feedstock, atmosphere, etc) and the resulted microstructures and mechanical properties. And it shows that appropriate process parameters can significantly reduce the microstructural defects and improve the mechanical properties. Since the process parameters in the process are various and interdependent, for each SLM material process is not fully optimized and future work is needed to obtain the optimum parameters to meet its specific requirements.

- *Support structure design*: Support structure is required in the SLM process for both supporting the overhanging parts and minimizing the thermal stress-induced geometrical distortions. Therefore, support structure strategy could significantly affect the process stability, building time, post support structure-removal work and surface finish. So far, the research on the support structure design or optimization accounts for a small part of the SLM work, possibly due to the fact that the current focus is placed on the process-microstructure-properties research. To further implement of complex-geometry components in SLM, designing the support structure and developing the support strategy would deserve more future work.

Electron beam melting & selective laser melting IN718

The materials involved in this licentiate research include both EBM IN718 and SLM IN718. Given the EBM and SLM processes were reviewed in a general sense in Chapter 3 and 4, a more specific review on the microstructures and mechanical properties of EBM IN718 and SLM IN718 is provided in this chapter. The idea here is not to compare one's superiority to the other, but instead to identify the missing/controversial part in the published literatures, based on which this licentiate research is guided to solve these problems.

5.1 EBM IN718

Strondl et al. [74] reported the very first research on EBM IN718. This as-manufactured EBM IN718 has the γ grains elongated along the building direction and $\langle 100 \rangle$ $/\!/$ building direction texture. The strengthening precipitate γ'' has precipitated in the γ matrix, and small (Ti,Nb)(C,N,B) precipitates can be found to string and align parallel to the building direction. In their subsequent paper [75], anisotropic tensile properties were reported as due to the local agglomerate of porosities rather than the intrinsic properties. The anisotropic tensile properties were further confirmed by Kirka et al. [77, 186]: both the tensile strength and elongation are higher tested along the building direction that tested perpendicular to the building direction in the as-manufactured sample, and these anisotropic properties almost disappear after post heat-treatment. The microstructure gradient along the building direction was first reported by Unocic et al. [187], and was attributed to the height-dependant thermal exposure experienced by different parts of the component [61]. The strength is correspondingly gradient, namely progressively increased tensile strength and elongation with the distance from the bottom, which is associated with the decomposition of γ'' and precipitation of δ.

An *in situ* controlled heat treatment was attempted, by scanning the top surface of the build after the process was finished, to homogenize and age the microstructure, but resulted in cracks and poor tensile performance [188]. Efforts have also been put in identifying process-microstructure relationship, showing that besides the higher density and better surface finish, the controlled tailoring of grain structures and crystallographic textures can be achieved by adjusting the scan strategies [62, 76, 78, 189, 190].

5.2 SLM IN718

Amato et al. [191] performed the pioneering microstructure and mechanical behaviour characterizations on SLM IN718, and found that the strengthening phase γ'' is present in the as-manufactured SLM IN718. Differently, the subsequently published TEM work by Zhang et al. [163] and Choi et al. [192] showed that the as-manufactured SLM IN718 has very few γ'/γ'' precipitated in matrix due to the high temperature gradient and rapid solidification rate, but instead large amount of fine Laves phases and carbides can be found as well as dislocation sub-grain structures. The as-manufactured SLM IN718 is mostly associated with lower strengthen than after being heat-treated (solution+ageing or direct ageing) [160, 161, 163, 166, 193–195], during which the strengthening phases γ'/γ'' precipitate and strengthen the matrix. Optimizing the heat treatments have been performed to dissolve the Laves phase and correctly precipitate the δ and strengthening phases γ'/γ''. Higher homogenization/solution temperature or longer homogenization/solution holding time is necessary for removing the Nb segregation and improving mechanical properties [163, 166]. The texture in the as-manufactured SLM IN718 can vary with the specific process parameters. Both strong $\langle 001 \rangle \parallel$ building direction texture [160, 167, 194] and relatively isotropic crystallographic orientations [165, 195, 196] have been reported. Besides the microstructure characterizations, focus is also put on the building orientation dependency of mechanical properties. Though the mechanical properties largely depend on the specific process parameters, the general trends and observations are common to all SLM IN718 builds: the horizontally built samples have slightly higher tensile strength than the vertically built samples [160, 164, 166, 194, 195].

Experimental methods

The experimental methods used in the research of this thesis will be present in this chapter. The EBM IN718 materials were provided by Sandvik Machining Solutions AB, Sweden, and the SLM IN718 materials were provided by Siemens AG, Germany. The post heat treatments, metallographic preparations, microstructure characterizations, tensile tests and hardness measurements were performed at Linköping University.

6.1 Materials

6.1.1 EBM IN718

The EBM IN718 was manufactured with an Arcam A2X EBM machine at Sandvik Machining Solutions AB. The powders used were plasma atomized, with nominal size ranging from 25 to 106 μm. The chemical composition is given in Table 6.1. The process parameters were set as suggested by Arcam AB, and the powder bed temperature (measured from the base plate) was kept at about 1020 °C throughout the process. The manufacturing batch contained 16 identical blocks. Each block is dimensioned as in Fig. 6.1a. Note that all these blocks were provided in the as-manufactured condition, directly removing from the base plate without any treatment. For more information about this process please refer to appended paper I.

6.1.2 SLM IN718

Gas atomized IN718 powders with the nominal size less than 65 μm were used as the raw material for the SLM process. The nominal chemical composition of the
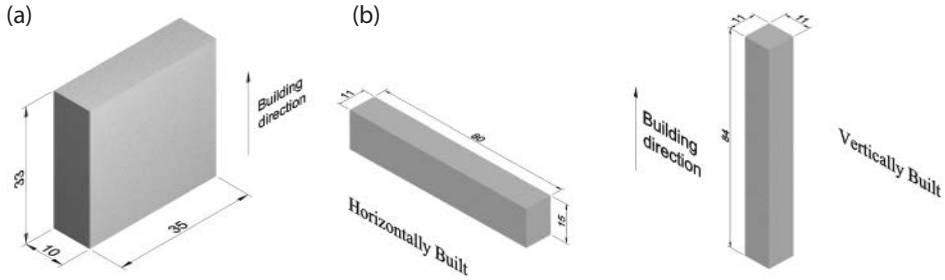
Figure 6.1. Schematics of as-manufactured (a) EBM IN718 and (b) SLM IN718 blocks.

Table 6.1. Nominal chemical composition of the Arcam plasma atomized IN718 powder

Element	Ni	Cr	Fe	Nb	Mo	Co	Ti	Al
wt.%	Bal.	19.1	18.5	5.04	2.95	0.07	0.91	0.58
Element	Mn	Si	Cu	C	P	S	N	O
wt.%	0.05	0.13	0.1	0.035	0.004	0.001	0.0128	0.0133

gas atomized IN718 powder is given in Table 6.2. All the samples were manufactured with an EOS M290 machine equipped with a maximum 400 W Yb-fiber laser. The process parameters were as recommended by EOS. The components' longitude directions are either parallel to or perpendicular to the base plate, designating as horizontally built and vertically built, respectively. The dimensions are as shown in Fig. 6.1b. Note that all these blocks were provided in the as-manufactured condition, directly removing from the base plate without any treatment. For more information about this process please refer to appended paper III.

Table 6.2. Nominal chemical composition of the gas atomized IN718 powder

Element	Ni	Cr	Fe	Nb	Mo
wt.%	50~55	17.0~21.0	Bal.	4.75~5.5	2.8~3.3
Element	Co	Ti	Al	Mn	Si
wt.%	<1.0	0.65~1.15	0.20~0.80	<0.35	<0.35
Element	Cu	C	P	S	B
wt.%	<0.3	<0.08	<0.015	<0.0015	<0.006

6.2 Microstructure characterization

6.2.1 Metallographic preparation

For scanning electron microscopy characterization, samples were cut at the interested plane and mounted, then mechanically grinded successively from 500 Grit

to 4000 Grit, and polished with diamond suspension from 3 μm to 1/4 μm and finally with OP-U colloidal silica suspension. Specifically for the SLM IN718, to reveal the dendritic microstructure, the polished samples were etched for a few seconds using a 10 ml hydrochloric acid + 1.5 ml 30% hydrogen peroxide etchant. For transmission electron microscopy characterization, thin foil samples were prepared by mechanically grinding down to 50 μm. To further thin down to electron transparent, electropolishing was conducted in 10 vol.% perchloric acid + 90 vol.% Ethanol electrolyte at -20 °C with a Struers TenuPol-5 electrolytic machine, or ion milling was performed with a Gatan 691 Precision Ion Polishing system.

6.2.2 Scanning electron microscopy

A Hitachi SU70 FEG scanning electron microscope (SEM) equipped with energy dispersive X-ray spectroscopy (EDS) and electron back scatter diffraction (EBSD) system from Oxford Instrument, was operated at 20 KV for microstructure characterization.

6.2.3 Transmission electron microscopy

The transmission electron microscopy (TEM) characterization was performed using a FEI Tecnai G2 TEM, operating at an accelerating voltage of 200 kV. A double tilt holder was used for all the TEM experiments to tilt the sample to desired zone axis for better imaging.

6.2.4 Residual stress measurement

Residual stress measurements were performed on a four-circle Seifert X-ray diffractometer equipped with a CrK_α radiation and a linear position-sensitive detector. Two in-plane stresses were measured on the as-manufactured sample surface. The diffraction angle was chosen at $2\theta \sim 128°$ for the {220} plane family to have high angel diffraction peak, and $sin^2\psi$ method with an X-ray elastic constant of 4.65×10^{-6} MPa^{-1} [197] was chosen to calculate the residual stress.

6.3 Mechanical test

6.3.1 Hardness test

A Struers DuraScan G5 hardness tester was used to measured the vickers microhardness with 300 g load and 15 s dwell-time. For each sample no less than 20 indentations were performed to get good statistics.

6.3.2 Tensile test

Tensile test samples were electrical discharge machined with reference to the building orientation, namely parallel/perpendicular to the building direction, to investigate the sample orientation dependency of tensile properties. For the geometries

of tensile test samples please refer to the appended papers. 3∼4 samples were tested per test condition to obtain acceptable statistics. Tensile tests were conducted under room temperature and open air, using an Instron 5582 universal test machine with a 100 kN load cell and at a 0.10 %/s strain rate. Since the test sample was too small to measure strain with extensometer, the strain was measured using a digital image correlation (DIC) system from Image System AB.

Summary of included papers

The following papers have been included in this Licentiate thesis.

   I D. Deng, J. Moverare, R. L. Peng, H. Söderberg (2017). Microstructure and anisotropic mechanical properties of EBM manufactured Inconel 718 and effects of post heat treatments. Materials Science and Engineering: A, 693, 151-163.

  II D. Deng, J. Moverare, R. L. Peng, H. Söderberg (2018). Height dependent microstructure in Inconel 718 manufactured by Electron Beam Melting. *In manuscript*

III D. Deng, R. L. Peng, H. Brodin, J. Moverare (2018). Microstructure and mechanical properties of Inconel 718 produced by selective laser melting: Sample orientation dependence and effects of post heat treatments. Materials Science and Engineering: A, 713, 294-306.

Paper I

Microstructure and anisotropic mechanical properties of EBM manufactured Inconel 718 and effects of post heat treatments

    This paper is partly motivated to investigate the microstructures corresponding to contour and hatching regions and the mechanisms behind the anisotropic mechanical properties. Tuning the post heat treatment with comparison to the AMS 5662 specification is also of interested.

    The contour microstructure is characterized as heterogeneous grain morphologies and the overall weak texture, while the hatch region is mostly coarse columnar

grains elongated along the building direction and has strong $\langle 001 \rangle \parallel$ building direction texture. The anisotropic tensile properties are observed as higher tensile strength but lower elongation along the building direction than normal to the building direction. However, the anisotropy does not seem to result from the $\langle 001 \rangle \parallel$ building direction texture, but instead is possibly attributed to the alignment and distribution of porosities. Since the as-manufactured microstructure has already be strengthened by the strengthening phases γ'/γ'', heat treatments just slightly increase the strength, and the direct ageing without solution treatment seems to be the optimum post heat treatment.

Paper II

Height dependent microstructure in Inconel 718 manufactured by Electron Beam Melting

This paper is a sequel of the first paper, with focus on characterizing the as-manufactured microstructure gradient along the building direction and rationalizing the phase evolution during the complex thermal cycles.

Due to the relatively high powder bed temperature and the injection of helium to facilitate cooling after the building process, the as-manufactured IN718 shows a microstructure gradient: from the top surface towards the bottom, the Laves phase volume fraction increases from about zero, peaks to about 2.3% at 150 μm from the top surface, and decreases gradually to zero again at 1800 μm from the top surface. The quenched, as-solidified and as-homogenized microstructures are distinguished within the as-manufactured microstructure. Based on that, the formation of Laves phase is rationalized with the low cooling rate enabling the considerable segregation of Nb, which is contradictory to the generally rapid solidification reported in the literatures. 40 minutes of "in-situ" homogenization, namely soaking in the powder bed before helium is injected, is able to dissolute completely the Laves phase in as-solidified condition and redistribute homogeneously Nb within the matrix. Exceptionally, absence of Laves phase close to the top surface is attributed to the rapid solidification caused by helium quenching. Carbide/nitride/carbonitride is less affected by the complex thermal history due to their highly stability. δ phase is expected to precipitate during the cooling stage, showing similar evolution as Laves phase. The cooling condition of the cooling stage also favours the precipitation of γ'/γ'' throughout the sample, and yields considerably high strength in the as-manufactured condition.

Paper III

Microstructure and mechanical properties of Inconel 718 produced by selective laser melting: Sample orientation dependence and effects of post heat treatments

A aim of this paper is to optimize the post heat treatment for SLM IN718, regarding to homogenizing the segregation and correctly precipitating the strengthening phases for peak strength. Also this paper is also motivated to uncover the

mechanisms for the "isotropic crystallographic orientations but anisotropic mechanical properties" behaviour.

The as-manufactured SLM IN718 has a very fine cellular-dendritic structure, with numbers of fine Laves phases precipitating in the interdendritic region and relatively weak texture. Though no strengthening phases γ'/γ'' precipitated in the as-manufactured condition, the strength is still higher than that of fully solution treated condition reported in the literature, due to the "work-hardening" by residual strain/dislocation. The horizontally built samples have higher tensile strength but lower elongation than the vertically built samples. These anisotropic tensile properties are mainly attributed to the different amounts of residual stress accumulated, with increasing the heat treatment temperature or duration the differences of tensile properties are minimized. By comparing the heat treatments applied in the present paper, the post heat treatment can be optimized by prolonging the homogenization duration at 1080 °C but reducing the holding time of solution at 980 °C.

Conclusion

The research present in this licentiate thesis focuses on the microstructures and mechanical properties of IN718 manufactured by EBM and SLM. By addressing the research questions as mentioned in Chapter *Introduction*, the following conclusions can be made:

For EBM IN718:

- The as-manufactured microstructure is not homogeneous, but instead is location-dependent. The grains in the frame part of the build are rather irregular and show very weak texture, while the core part of the build has mostly coarse columnar grains elongated along the building direction and strong $\langle 001 \rangle \parallel$ building direction texture. And due to the relatively hight chamber temperature throughout the building process, the previously deposited layers experience longer "*in-situ* annealing" than the subsequently deposited layers. Certain amount of helium is also used to accelerate the cooling when the process is finished. Given that, the segregation of Nb and precipitation of Laves phases are present in an "increasing from zero and then decreasing subsequently to zero again" manner from the top surface towards the bottom.

- The tensile test shows higher tensile strength but lower elongation along the building direction than perpendicular to the building direction. The anisotropy results possibly from the alignment of porosities rather than the texture.

- Applying heat treatment does not significantly increase the strength since the strengthening phases γ'/γ'' have already precipitated in the as-manufactured condition. Currently, the direct ageing treatment seems to be the optimum

for the part free of segregation and Laves phase, while for the whole build future work is needed to optimize the heat treatment due to the segregation and Laves phase near the top surface.

For SLM IN718:

- The as-manufactured SLM IN718 has very fine dendritic microstructure and weak texture, with very fine Laves phase in the interdendrites and without strengthening phases γ'/γ'' in the matrix.

- The different accumulations of residual stress are responsible for the "anisotropic"/sample orientation dependent tensile properties, namely the horizontally built samples have higher strength but lower elongation than the vertically build samples.

- Heat treatment is necessary to homogenize the segregation and correctly precipitate the strengthening phases γ'/γ''. With increasing the heat treatment temperature or holding time the "anisotropy" decreases.

Given this research involves both EBM IN718 and SLM IN718, a comparison between the microstructures and mechanical properties would be of interest, which would provide a better overview of both processes. A brief comparison, based on **as-manufactured** microstructural and mechanical features, is summarized in the Table 8.1.

Table 8.1. Comparisons of as-manufactured EBM IN718 and SLM IN718 on microstructural and mechanical features

		EBM IN718	SLM 718
Microstructure	Grain Morphology	Columnar, elongated along BD, can up to millimeter	Irregular, a few hundred microns
	Texture	Strong $\langle 100 \rangle$ // BD	Non-textured
	Homogenity	Microstructure gradient near the top surface	Homogeneous throughout the sample
	Precipitate	γ'/γ'', δ, carbide/nitride/carbonitride, Laves (just present near the top surface)	Laves
Mechanical property	Hardness	$\sim$ HV$_{0.3}$ 428	$\sim$ HV$_{0.3}$ 325
	Tensile Aniostropy	Yes	Yes
	Tensile strength	// BD: 1113 MPa, $\perp$ BD: 1002 MPa	// BD: 989 MPa, $\perp$ BD: 1068 MPa
	Elongation	// BD: 31 %, $\perp$ BD: 40 %	// BD: 35 %, $\perp$ BD: 31 %
	Tensile properties deviation	EBM samples have larger deviation than SLM samples	
	Strengthening mechanism	by γ'/γ''	by residual strain and dislocations
Surface roughness		SLM samples have better surface roughness than EBM samples	

- The microstructural and mechanical features of EBM IN718 in this table are specifically from the **hatch** region.

- Denotation: // means parallel to, $\perp$ means perpendicular to, BD means building direction.

CHAPTER 9

Future work

This licentiate thesis serves as a midterm summary and reflection of the research progress during the past 2.5 years, as well as a foundation for the next phase of my Ph.D. journey. Focus will be still on both the EBM IN718 and SLM IN718, but might shift from the microstructure characterizations and monotonic mechanical properties to the cyclic mechanical properties, since most of the IN718 applications involve cyclic loadings.

As indicated in the appended papers, the as-manufactured sample is not at the peak aged condition, which needs heat treatment improve the strength, for both EBM and SLM IN718. Heat treatment can significantly affect the precipitation or dissolution of certain precipitates. The effects of precipitates on fatigue crack propagation behaviours are of interest, but so far have been rarely reported. On the other hand, specifically for EBM IN718, the columnar grain boundaries are mostly parallel to the building direction, and the grain boundaries' role on crack propagation would be studied under loading that is either parallel or perpendicular to building direction.

4-point bending fatigue test is also planned to investigate the crack initiation behaviours on machined samples at HIPed and un-HIPed, heat treated and un-heat treated conditions for both EBM and SLM IN718.

Bibliography

[1] W. J. Sames, F. A. List, S. Pannala, R. R. Dehoff, and S. S. Babu. "The metallurgy and processing science of metal additive manufacturing". In: *International Materials Reviews* 61.5 (2016), pp. 315–360.

[2] Daniel F. Paulonis and John J. Schirra. "Alloy 718 at Pratt & Whitney– Historical perspective and future challenges". In: *Superalloys 718,625,706* (2001), pp. 13–23.

[3] Roger C Reed. *The superalloys: fundamentals and applications*. Cambridge university press, 2008.

[4] J. W. Brooks and P. J. Bridges. "Metallurgical stability of Inconel alloy 718". In: *Superalloys 1988*. Ed. by S. Reichman, D. N. Duhl, G. Manurer, S. Antolovich, and C. Lund. 1988, pp. 33–42.

[5] Edward A Loria. "The status and prospects of alloy 718". In: *JOM Journal of the Minerals, Metals and Materials Society* 40.7 (1988), pp. 36–41.

[6] Sarwan K. Mannan et al. "Alloy 718 for oilfield applications". In: *JOM* 64.2 (2012), pp. 265–270.

[7] Matthew J Donachie and Stephen J Donachie. *Superalloys: a technical guide*. ASM international, 2002.

[8] Randy Bowman. "Superalloys: A primer and history". In: *9th International Symposium on superalloys*. 2000.

[9] A. J. Ardell. "Order hardening: comparison between revised theory and experiment". In: *Metal Science* 14.6 (1980), pp. 221–224.

[10] M. C. Chaturvedi and Ya-fang Han. "Strengthening mechanisms in Inconel 718 superalloy". In: *Metal science* 17.3 (1983), pp. 145–149.

[11] Kiyoshi Kusabiraki, Shuuichi Ikeuchi, and Takayuki Ooka. "Morphology and Lattice Constants of γ'' Precipitates in a Ni–18Cr–16Fe–5Nb–3Mo Alloy". In: *Materials Transactions, JIM* 37.5 (1996), pp. 1050–1055.

[12] J. M. Oblak, D. F. Paulonis, and D. S. Duvall. "Coherency strengthening in Ni base alloys hardened by DO_{22} γ' precipitates". In: *Metallurgical and Materials Transactions B* 5.1 (1974), pp. 143–153.

[13] D. F. Paulonis, J. M. Oblak, and D. S. Duvall. *Precipitation in Nickel-base alloy 718*. Tech. rep. Pratt and Whitney Aircraft, Middletown, Conn., 1969.

[14] R. B. Li, M. Yao, W. C. Liu, and X. C. He. "Isolation and determination for δ, γ' and γ'' phases in Inconel 718 alloy". In: *Scripta Materialia* 46.9 (2002), pp. 635–638.

[15] Alexandre Devaux, Loic Nazé, Régine Molins, André Pineau, A Organista, J. Y. Guédou, J. F. Uginet, and P. Héritier. "Gamma double prime precipitation kinetic in Alloy 718". In: *Materials Science and Engineering: A* 486.1 (2008), pp. 117–122.

[16] Saied Azadian, Liu-Ying Wei, and Richard Warren. "Delta phase precipitation in Inconel 718". In: *Materials characterization* 53.1 (2004), pp. 7–16.

[17] W. D. Cao and R. Kennedy. "Role of chemistry in 718-type alloys–Allvac® 718Plus alloy development". In: *Superalloys 2004* (2004), pp. 91–99.

[18] Xishan Xie, Jianxin Dong, Gailian Wang, Wei You, Jinhui Du, Changhong Zhao, and Zhigang Wang. "The effect of Nb, Ti, Al on precipitation and strengthening behavior of 718 type superalloys". In: *Superalloys* 718 (2005), pp. 625–706.

[19] John P. Collier, Song How Wong, John K. Tien, and James C. Phillips. "The effect of varying AI, Ti, and Nb content on the phase stability of Inconel 718". In: *Metallurgical and Materials Transactions A* 19.7 (1988), pp. 1657–1666.

[20] Y. Desvallées, M. Bouzidi, F. Bois, and N. Beaude. "Delta pahse in Inconel 718: Mechanical properties and forging process requirements". In: *Superalloys 718, 625, 706 and various derivatives* 718 (1994), p. 281.

[21] Shuqi Li, J. Y. Zhuang, J. Y. Yang, and X. S. Xie. "The effect of phase on crack propagation under creep and fatigue conditions in alloy 718". In: *Superalloys 718, 625, 706 and various derivatives* 718 (1994), pp. 625–706.

[22] B. Pieraggi and J. F. Uginet. "Fatigue and creep properties in relation with Alloy 718 microstructure". In: *Superalloys 718, 625, 706 and various derivatives* 718 (1994), pp. 535–544.

[23] D. Gopikrishna, S. N . Jha, and L. N. Dash. "Influence of microstructure on fatigue properties of Alloy 718". In: *The Fourth International Special Emphasis Symposium on Superalloy, Pittsburgh, Pennsylvania*. 1997.

[24] J. P. Pedron and A. Pineau. "The effect of microstructure and environment on the crack growth behaviour of Inconel 718 alloy at 650 °C under fatigue, creep and combined loading". In: *Materials science and engineering* 56.2 (1982), pp. 143–156.

[25] B. Hong, X. Yi, and Q. Meng. "Effect of delta-Ni$_3$Nb on low cycle fatigue fracture of Inconel 718". In: *Acta Metallurgica Sinica(China)(People's Republic of China)* 27.1 (1991).

[26] M. Sundararaman, P. Mukhopadhyay, and S. Banerjee. "Carbide precipitation in nickel base superalloys 718 and 625 and their effect on mechanical properties". In: *Superalloys* 718 (1997), pp. 625–706.

[27] Blaine Geddes, Hugo Leon, and Xiao Huang. *Superalloys: alloying and performance.* Asm International, 2010.

[28] A. Mitchell, A. J. Schmalz, C. Schvezov, and S. Cockroft. "The precipitation of primary carbides in Alloy 718". In: *Superalloys* 718.625,706 (1994), pp. 65–78.

[29] John F. Radavich. "The physical metallurgy of cast and wrought alloy 718". In: *Conference Proceedings on Superalloy.* Vol. 718. 1989, pp. 229–240.

[30] M. J. Cieslak, G. A. Knorovsky, T. J. Headley, and A. D. Romig Jr. "The solidification metallurgy of alloy 718 and other Nb-containing superalloys". In: *Superalloy* 718 (1989), pp. 59–68.

[31] Keh-Minn Chang, Hong-Jen Lai, and Jeng-Ying Hwang. "Existence of Laves phase in Nb-hardened superalloys". In: *Superalloys 718, 625, 706 and various derivatives* (1994), pp. 683–694.

[32] John J. Schirra, Robert H. Caless, and Robert W. Hatala. "The effect of Laves phase on the mechanical properties of wrought and cast+ HIP Inconel 718". In: *Superalloys* 718.625 (1991), pp. 375–388.

[33] N. L. Richards, X. Huang, and M. C. Chaturvedi. "Heat affected zone cracking in cast Inconel 718". In: *Materials characterization* 28.4 (1992), pp. 179–187.

[34] Yunpeng Mei, Yongchang Liu, Chenxi Liu, Chong Li, Liming Yu, Qianying Guo, and Huijun Li. "Effect of base metal and welding speed on fusion zone microstructure and HAZ hot-cracking of electron-beam welded Inconel 718". In: *Materials & Design* 89 (2016), pp. 964–977.

[35] G. A. Knorovsky, M. J. Cieslak, T. J. Headley, A. D. Romig, and W. F. Hammetter. "Inconel 718: a solidification diagram". In: *Metallurgical Transactions A* 20.10 (1989), pp. 2149–2158.

[36] T. Antonsson and H. Fredriksson. "The effect of cooling rate on the solidification of Inconel 718". In: *Metallurgical and Materials Transactions B* 36.1 (2005), pp. 85–96.

[37] A. Mitchell. "The Precipitation of Primary Carbides in IN718 and Its Relation to Solidification Conditions". In: *Superalloys 718, 625, 706 and Derivatives* (2005), pp. 299–310.

[38] Tresa M. Pollock and Sammy Tin. "Nickel-based superalloys for advanced turbine engines: chemistry, microstructure, and properties". In: *Journal of propulsion and power* 22.2 (2006), pp. 361–374.

[39]   R. G. Carlson and J. F. Radavich. "Microstructural characterization of cast 718". In: *International Symposium on Superalloys*. 1989.

[40]   Zhang Maicang, Cao Guoxin, Dong Jianxin, Zheng Lei, and Yao Zhihao. "Investigations on dissolution mechanism of Laves phase in GH4169 alloy ingot based on classic dynamic model". In: *Acta Metallurgica Sinica* 49.3 (2013), pp. 372–378.

[41]   G. Appa Rao, Mahendra Kumar, M. Srinivas, and D. S. Sarma. "Effect of standard heat treatment on the microstructure and mechanical properties of hot isostatically pressed superalloy Inconel 718". In: *Materials Science and Engineering: A* 355.1 (2003), pp. 114–125.

[42]   G. Appa Rao, M. Srinivas, and D. S. Sarma. "Effect of oxygen content of powder on microstructure and mechanical properties of hot isostatically pressed superalloy Inconel 718". In: *Materials Science and Engineering: A* 435 (2006), pp. 84–99.

[43]   G. Appa Rao, M. Srinivas, and D. S. Sarma. "Influence of modified processing on structure and properties of hot isostatically pressed superalloy Inconel 718". In: *Materials Science and Engineering: A* 418.1 (2006), pp. 282–291.

[44]   Arcam EBM. *Arcam History*. http://www.arcam.com/company/about-arcam/history.

[45]   C. Körner. "Additive manufacturing of metallic components by selective electron beam melting - a review". In: *International Materials Reviews* 61.5 (2016), pp. 361–377.

[46]   Arcam EBM. *Arcam Brochure*. http://www.arcam.com/wp-content/uploads/arcamebm-corp.pdf.

[47]   M. Kahnert, S. Lutzmann, and M. F. Zaeh. "Layer formations in electron beam sintering". In: *Solid freeform fabrication symposium*. 2007, pp. 88–99.

[48]   Chao Guo, Wenjun Ge, and Feng Lin. "Effects of scanning parameters on material deposition during Electron Beam Selective Melting of Ti-6Al-4V powder". In: *Journal of Materials Processing Technology* 217 (2015), pp. 148–157.

[49]   Arcam EBM. *EBM Hardware*. http://www.arcam.com/technology/electron-beam-melting/hardware/.

[50]   Arcam EBM. *Arcam Titanium Ti6Al4V powder*. http://www.arcam.com/wp-content/uploads/Arcam-Ti6Al4V-Titanium-Alloy.pdf.

[51]   L. E. Murr, E. V. Esquivel, S. A. Quinones, S. M. Gaytan, M. I. Lopez, E. Y. Martinez, F. Medina, D. H. Hernandez, E. Martinez, J. L. Martinez, et al. "Microstructures and mechanical properties of electron beam-rapid manufactured Ti–6Al–4V biomedical prototypes compared to wrought Ti–6Al–4V". In: *Materials characterization* 60.2 (2009), pp. 96–105.

[52] Joakim Karlsson, Anders Snis, Håkan Engqvist, and Jukka Lausmaa. "Characterization and comparison of materials produced by Electron Beam Melting (EBM) of two different Ti–6Al–4V powder fractions". In: *Journal of Materials Processing Technology* 213.12 (2013), pp. 2109–2118.

[53] W. J. Sames, F. Medina, W. H. Peter, S. S. Babu, and R. R. Dehoff. "Effect of process control and powder quality on Inconel 718 produced using electron beam melting". In: *8th International Symposium on Superalloy 718 and Derivatives*. John Wiley & Sons, Inc. 2014, pp. 409–423.

[54] Xiaoming Zhao, Jing Chen, Xin Lin, and Weidong Huang. "Study on microstructure and mechanical properties of laser rapid forming Inconel 718". In: *Materials Science and Engineering: A* 478.1 (2008), pp. 119–124.

[55] H. Qi, M. Azer, and A. Ritter. "Studies of standard heat treatment effects on microstructure and mechanical properties of laser net shape manufactured Inconel 718". In: *Metallurgical and Materials Transactions A* 40.10 (2009), pp. 2410–2422.

[56] Jean-Pierre Kruth, Peter Mercelis, J Van Vaerenbergh, Ludo Froyen, and Marleen Rombouts. "Binding mechanisms in selective laser sintering and selective laser melting". In: *Rapid prototyping journal* 11.1 (2005), pp. 26–36.

[57] Hazman Hasib, Ola L. A. Harrysson, and Harvey A. West. "Powder removal from Ti-6Al-4V cellular structures fabricated via electron beam melting". In: *Jom* 67.3 (2015), pp. 639–646.

[58] S. S. Al-Bermani, M. L. Blackmore, W. Zhang, and I. Todd. "The origin of microstructural diversity, texture, and mechanical properties in electron beam melted Ti-6Al-4V". In: *Metallurgical and materials transactions a* 41.13 (2010), pp. 3422–3434.

[59] Peter Thomsen, Johan Malmström, Lena Emanuelsson, Magnus Rene, and Anders Snis. "Electron beam-melted, free-form-fabricated titanium alloy implants: Material surface characterization and early bone response in rabbits". In: *Journal of Biomedical Materials Research Part B: Applied Biomaterials* 90.1 (2009), pp. 35–44.

[60] H. K. Rafi, N. V. Karthik, Haijun Gong, Thomas L. Starr, and Brent E. Stucker. "Microstructures and mechanical properties of Ti6Al4V parts fabricated by selective laser melting and electron beam melting". In: *Journal of materials engineering and performance* 22.12 (2013), pp. 3872–3883.

[61] W. J. Sames, K. A. Unocic, R. R Dehoff, T. Lolla, and S. S. Babu. "Thermal effects on microstructural heterogeneity of Inconel 718 materials fabricated by electron beam melting". In: *Journal of Materials Research* 29.17 (2014), pp. 1920–1930.

[62] Harald Ernst Helmer, Carolin Körner, and Robert Friedrich Singer. "Additive manufacturing of nickel-based superalloy Inconel 718 by selective electron beam melting: Processing window and microstructure". In: *Journal of Materials Research* 29.17 (2014), pp. 1987–1996.

[63] Nikolas Hrabe, Thomas Gnäupel-Herold, and Timothy Quinn. "Fatigue properties of a titanium alloy (Ti–6Al–4V) fabricated via electron beam melting (EBM): Effects of internal defects and residual stress". In: *International Journal of Fatigue* 94 (2017), pp. 202–210.

[64] Joakim Karlsson, Mats Norell, Ulf Ackelid, Håkan Engqvist, and Jukka Lausmaa. "Surface oxidation behavior of Ti–6Al–4V manufactured by Electron Beam Melting (EBM®)". In: *Journal of Manufacturing Processes* 17 (2015), pp. 120–126.

[65] Xibing Gong, Bo Cheng, Steven Price, and Kevin Chou. "Powder-bed electron-beam-melting additive manufacturing: powder characterization, process simulation and metrology". In: *Proceedings of the ASME District F Early Career Technical Conference*. 2013, pp. 59–66.

[66] Alphons Anandaraj Antonysamy, J. Meyer, and P. B. Prangnell. "Effect of build geometry on the β-grain structure and texture in additive manufacture of Ti 6Al 4V by selective electron beam melting". In: *Materials characterization* 84 (2013), pp. 153–168.

[67] Dunyong Deng, Johan Moverare, Ru Lin Peng, and Hans Söderberg. "Microstructure and anisotropic mechanical properties of EBM manufactured Inconel 718 and effects of post heat treatments". In: *Materials Science and Engineering: A* 693 (2017), pp. 151–163.

[68] S. M. Gaytan, L. E. Murr, F. Medina, E. Martinez, M. I. Lopez, and R. B. Wicker. "Advanced metal powder based manufacturing of complex components by electron beam melting". In: *Materials Technology* 24.3 (2009), pp. 180–190.

[69] M. Svensson, U. Ackelid, and A. Ab. "Titanium alloys manufactured with electron beam melting mechanical and chemical properties". In: *Proceedings of the Materials and Processes for Medical Devices Conference*. ASM International. 2010, pp. 189–194.

[70] M. Kahlin, H. Ansell, and J.J. Moverare. "Fatigue behaviour of additive manufactured Ti6Al4V, with as-built surfaces, exposed to variable amplitude loading". In: *International Journal of Fatigue* 103 (2017), pp. 353–362.

[71] Mohsen Seifi, Ayman Salem, Daniel Satko, Joshua Shaffer, and John J Lewandowski. "Defect distribution and microstructure heterogeneity effects on fracture resistance and fatigue behavior of EBM Ti–6Al–4V". In: *International Journal of Fatigue* 94 (2017), pp. 263–287.

[72] S. Leuders, M . Thöne, A. Riemer, T. Niendorf, T. Tröster, H. A. Richard, and H. J. Maier. "On the mechanical behaviour of titanium alloy TiAl6V4 manufactured by selective laser melting: Fatigue resistance and crack growth performance". In: *International Journal of Fatigue* 48 (2013), pp. 300–307.

[73] Adnan Safdar, H. Z. He, Liu-Ying Wei, A. Snis, and Luis E. Chavez de Paz. "Effect of process parameters settings and thickness on surface roughness of EBM produced Ti-6Al-4V". In: *Rapid Prototyping Journal* 18.5 (2012), pp. 401–408.

[74] A. Strondl, R. Fischer, G. Frommeyer, and A. Schneider. "Investigations of MX and γ /γ precipitates in the nickel-based superalloy 718 produced by electron beam melting". In: *Materials Science and Engineering: A* 480.1 (2008), pp. 138–147.

[75] A. Strondl, M. Palm, J. Gnauk, and G. Frommeyer. "Microstructure and mechanical properties of nickel based superalloy IN718 produced by rapid prototyping with electron beam melting (EBM)". In: *Materials Science and Technology* 27.5 (2011), pp. 876–883.

[76] Carolin Körner, Harald Helmer, Andreas Bauereiß, and Robert F. Singer. "Tailoring the grain structure of IN718 during selective electron beam melting". In: *MATEC Web of Conferences*. Vol. 14. EDP Sciences. 2014, p. 08001.

[77] M. M. Kirka, K. A. Unocic, N. Raghavan, F. Medina, R. R. Dehoff, and S. S. Babu. "Microstructure development in electron beam-melted Inconel 718 and associated tensile properties". In: *JOM* 68.3 (2016), pp. 1012–1020.

[78] H. Helmer, A. Bauereiß, R. F. Singer, and C. Körner. "Grain structure evolution in Inconel 718 during selective electron beam melting". In: *Materials Science and Engineering: A* 668 (2016), pp. 180–187.

[79] K. N. Amato, J. Hernandez, L. E. Murr, E. Martinez, S. M. Gaytan, P. W. Shindo, and S. Collins. "Comparison of microstructures and properties for a Ni-base superalloy (alloy 625) fabricated by electron beam melting". In: *Journal of Materials Science Research* 1.2 (2012), p. 3.

[80] Shuai Li, Qingsong Wei, Yusheng Shi, Zicheng Zhu, and Danqing Zhang. "Microstructure characteristics of Inconel 625 superalloy manufactured by selective laser melting". In: *Journal of Materials Science & Technology* 31.9 (2015), pp. 946–952.

[81] L. E. Murr, E. Martinez, X. M. Pan, S. M. Gaytan, J. A. Castro, C. A. Terrazas, F. Medina, R. B. Wicker, and D. H. Abbott. "Microstructures of Rene 142 nickel-based superalloy fabricated by electron beam melting". In: *Acta Materialia* 61.11 (2013), pp. 4289–4296.

[82] Markus Ramsperger, Robert F. Singer, and Carolin Körner. "Microstructure of the Nickel-Base superalloy CMSX-4 fabricated by selective electron beam melting". In: *Metallurgical and Materials Transactions A* 47.3 (2016), pp. 1469–1480.

[83] Al Marti. "Cobalt-base alloys used in bone surgery". In: *Injury* 31 (2000), pp. D18–D21.

[84] Clémence Petit, Eric Maire, Sylvain Meille, Jérôme Adrien, Shingo Kurosu, and Akihiko Chiba. "CoCrMo cellular structures made by Electron Beam Melting studied by local tomography and finite element modelling". In: *Materials Characterization* 116 (2016), pp. 48–54.

[85] Kevin Hazlehurst, Chang Jiang Wang, and Mark Stanford. "Evaluation of the stiffness characteristics of square pore CoCrMo cellular structures manufactured using laser melting technology for potential orthopaedic applications". In: *Materials & Design* 51 (2013), pp. 949–955.

[86] Furqan A. Shah, Omar Omar, Felicia Suska, Anders Snis, Aleksandar Matic, Lena Emanuelsson, Birgitta Norlindh, Jukka Lausmaa, Peter Thomsen, and Anders Palmquist. "Long-term osseointegration of 3D printed CoCr constructs with an interconnected open-pore architecture prepared by electron beam melting". In: *Acta biomaterialia* 36 (2016), pp. 296–309.

[87] Xibing Gong, Ted Anderson, and Kevin Chou. "Review on powder-based electron beam additive manufacturing technology". In: *ASME/ISCIE 2012 international symposium on flexible automation.* American Society of Mechanical Engineers. 2012, pp. 507–515.

[88] Manuela Galati, Luca Iuliano, Alessandro Salmi, and Eleonora Atzeni. "Modelling energy source and powder properties for the development of a thermal FE model of the EBM additive manufacturing process". In: *Additive Manufacturing* 14 (2017), pp. 49–59.

[89] Joris Peels. *In 3D printing, what's the difference between selective laser sintering (SLS) and selective laser melting (SLM)?* https://www.quora.com/3D-Printing/In-3D-printing-whats-the-difference-between-selective-laser-sintering-SLS-and-selective-laser-melting-SLM.

[90] EOS. *Additive Manufacturing, Laser-Sintering and industrial 3D printing - Benefits and Functional Principle.* https://www.eos.info/additive_manufacturing/for_technology_interested.

[91] M . Shellabear and O. Nyrhilä. "DMLS-Development history and state of the art". In: *Laser Assisted Netshape Engineering 4, Proceedings of the 4th LANE* (2004), pp. 21–24.

[92] R. Morgan, C. J. Sutcliffe, and W. O'Neill. "Experimental investigation of nanosecond pulsed Nd: YAG laser re-melted pre-placed powder beds". In: *Rapid Prototyping Journal* 7.3 (2001), pp. 159–172.

[93] Isabel M. Martins, Luis Esperto, and Mário J. G. Santos. "Sintering M3/2 high speed steel powder by DMLS process". In: *Materials science forum.* Vol. 514. Trans Tech Publ. 2006, pp. 1506–1510.

[94] Bin Xiao and Yuwen Zhang. "Laser sintering of metal powders on top of sintered layers under multiple-line laser scanning". In: *Journal of Physics D: Applied Physics* 40.21 (2007), p. 6725.

[95] ISO. "ASTM 52900: 2015". In: *Additive manufacturing - general principles —terminology. London: BSI Standards Limited* (2016).

[96] Karolien Kempen, Bey Vrancken, Sam Buls, Lore Thijs, Jan Van Humbeeck, and Jean-Pierre Kruth. "Selective laser melting of crack-free high density M2 high speed steel parts by baseplate preheating". In: *Journal of Manufacturing Science and Engineering* 136.6 (2014), p. 061026.

[97] Hagedorn Yves-Christian, Wilkes Jan, Meiners Wilhelm, Wissenbach Konrad, and Poprawe Reinhart. "Net shaped high performance oxide ceramic parts by selective laser melting". In: *Physics Procedia* 5 (2010), pp. 587–594.

[98] Stijn Clijsters, Tom Craeghs, Sam Buls, Karolien Kempen, and Jean-Pierre Kruth. "In situ quality control of the selective laser melting process using a high-speed, real-time melt pool monitoring system". In: *The International Journal of Advanced Manufacturing Technology* 75.5-8 (2014), pp. 1089–1101.

[99] L. Parry, I. A. Ashcroft, and Ricky D. Wildman. "Understanding the effect of laser scan strategy on residual stress in selective laser melting through thermo-mechanical simulation". In: *Additive Manufacturing* 12 (2016), pp. 1–15.

[100] Il Hyuk Ahn, Seung Ki Moon, Jihong Hwang, and Guijun Bi. "Characteristic length of the solidified melt pool in selective laser melting process". In: *Rapid Prototyping Journal* 23.2 (2017), pp. 370–381.

[101] Michael F. Zaeh and Gregor Branner. "Investigations on residual stresses and deformations in selective laser melting". In: *Production Engineering* 4.1 (2010), pp. 35–45.

[102] Peter Mercelis and Jean-Pierre Kruth. "Residual stresses in selective laser sintering and selective laser melting". In: *Rapid Prototyping Journal* 12.5 (2006), pp. 254–265.

[103] Ahmed Hussein, Liang Hao, Chunze Yan, and Richard Everson. "Finite element simulation of the temperature and stress fields in single layers built without-support in selective laser melting". In: *Materials & Design* 52 (2013), pp. 638–647.

[104] Ina Yadroitsava, Stephen Grewar, Daniel Hattingh, and Igor Yadroitsev. "Residual stress in SLM Ti6Al4V alloy specimens". In: *Materials Science Forum*. Vol. 828. Trans Tech Publ. 2015, pp. 305–310.

[105] Igor Yadroitsev and Ina Yadroitsava. "Evaluation of residual stress in stainless steel 316L and Ti6Al4V samples produced by selective laser melting". In: *Virtual and Physical Prototyping* 10.2 (2015), pp. 67–76.

[106] Bey Vrancken, Ruben Wauthlé, Jean-Pierre Kruth, and Jan Van Humbeeck. "Study of the influence of material properties on residual stress in selective laser melting". In: *Proceedings of the solid freeform fabrication symposium*. 2013, pp. 1–15.

[107] Yang Liu, Yongqiang Yang, and Di Wang. "A study on the residual stress during selective laser melting (SLM) of metallic powder". In: *The International Journal of Advanced Manufacturing Technology* 87.1-4 (2016), pp. 647–656.

[108] Dong-Kyu Kim, Wanchuck Woo, Ji-Hyun Hwang, Ke An, and Shi-Hoon Choi. "Stress partitioning behavior of an AlSi10Mg alloy produced by selective laser melting during tensile deformation using in situ neutron diffraction". In: *Journal of Alloys and Compounds* 686 (2016), pp. 281–286.

[109] M. Shiomi, K. Osakada, K. Nakamura, T. Yamashita, and F. Abe. "Residual stress within metallic model made by selective laser melting process". In: *CIRP Annals-Manufacturing Technology* 53.1 (2004), pp. 195–198.

[110] Thomas Vilaro, Christophe Colin, Jean-Dominique Bartout, Loic Nazé, and Mohamed Sennour. "Microstructural and mechanical approaches of the selective laser melting process applied to a nickel-base superalloy". In: *Materials Science and Engineering: A* 534 (2012), pp. 446–451.

[111] Damien Buchbinder, Wilhelm Meiners, Norbert Pirch, Konrad Wissenbach, and Johannes Schrage. "Investigation on reducing distortion by preheating during manufacture of aluminum components using selective laser melting". In: *Journal of Laser Applications* 26.1 (2014), p. 012004.

[112] Jean-Pierre Kruth, Jan Deckers, Evren Yasa, and Ruben Wauthlé. "Assessing and comparing influencing factors of residual stresses in selective laser melting using a novel analysis method". In: *Proceedings of the institution of mechanical engineers, Part B: Journal of Engineering Manufacture* 226.6 (2012), pp. 980–991.

[113] Yanjin Lu, Songquan Wu, Yiliang Gan, Tingting Huang, Chuanguang Yang, Lin Junjie, and Jinxin Lin. "Study on the microstructure, mechanical property and residual stress of SLM Inconel-718 alloy manufactured by differing island scanning strategy". In: *Optics & Laser Technology* 75 (2015), pp. 197–206.

[114] Luke N. Carter, Christopher Martin, Philip J. Withers, and Moataz M. Attallah. "The influence of the laser scan strategy on grain structure and cracking behaviour in SLM powder-bed fabricated nickel superalloy". In: *Journal of Alloys and Compounds* 615 (2014), pp. 338–347.

[115] Bo Song, Xiao Zhao, Shuai Li, Changjun Han, Qingsong Wei, Shifeng Wen, Jie Liu, and Yusheng Shi. "Differences in microstructure and properties between selective laser melting and traditional manufacturing for fabrication of metal parts: A review". In: *Frontiers of Mechanical Engineering* 10.2 (2015), pp. 111–125.

[116] Lore Thijs, Frederik Verhaeghe, Tom Craeghs, Jan Van Humbeeck, and Jean-Pierre Kruth. "A study of the microstructural evolution during selective laser melting of Ti–6Al–4V". In: *Acta Materialia* 58.9 (2010), pp. 3303–3312.

[117]   Ruidi Li, Yusheng Shi, Zhigang Wang, Li Wang, Jinhui Liu, and Wei Jiang. "Densification behavior of gas and water atomized 316L stainless steel powder during selective laser melting". In: *Applied surface science* 256.13 (2010), pp. 4350–4356.

[118]   Ruidi Li, Jinhui Liu, Yusheng Shi, Li Wang, and Wei Jiang. "Balling behavior of stainless steel and nickel powder during selective laser melting process". In: *The International Journal of Advanced Manufacturing Technology* 59.9-12 (2012), pp. 1025–1035.

[119]   Nesma T Aboulkhair, Nicola M Everitt, Ian Ashcroft, and Chris Tuck. "Reducing porosity in AlSi10Mg parts processed by selective laser melting". In: *Additive Manufacturing* 1 (2014), pp. 77–86.

[120]   Jean-Pierre Kruth, Ludo Froyen, Jonas Van Vaerenbergh, Peter Mercelis, Marleen Rombouts, and Bert Lauwers. "Selective laser melting of iron-based powder". In: *Journal of Materials Processing Technology* 149.1 (2004), pp. 616–622.

[121]   Marleen Rombouts, Jean-Pierre Kruth, Ludo Froyen, and Peter Mercelis. "Fundamentals of selective laser melting of alloyed steel powders". In: *CIRP Annals-Manufacturing Technology* 55.1 (2006), pp. 187–192.

[122]   T. H. C. Childs, C. Hauser, and M. Badrossamay. "Selective laser sintering (melting) of stainless and tool steel powders: experiments and modelling". In: *Proceedings of the Institution of Mechanical Engineers, Part B: Journal of Engineering Manufacture* 219.4 (2005), pp. 339–357.

[123]   Evren Yasa and Jean-Pierre Kruth. "Microstructural investigation of Selective Laser Melting 316L stainless steel parts exposed to laser re-melting". In: *Procedia Engineering* 19 (2011), pp. 389–395.

[124]   Baicheng Zhang, Lucas Dembinski, and Christian Coddet. "The study of the laser parameters and environment variables effect on mechanical properties of high compact parts elaborated by selective laser melting 316L powder". In: *Materials Science and Engineering: A* 584 (2013), pp. 21–31.

[125]   Chunze Yan, Liang Hao, Ahmed Hussein, Philippe Young, and David Raymont. "Advanced lightweight 316L stainless steel cellular lattice structures fabricated via selective laser melting". In: *Materials & Design* 55 (2014), pp. 533–541.

[126]   Ruidi Li, Jinhui Liu, Yusheng Shi, Mingzhang Du, and Zhan Xie. "316L stainless steel with gradient porosity fabricated by selective laser melting". In: *Journal of Materials Engineering and Performance* 19.5 (2010), pp. 666–671.

[127]   Thomas Niendorf, Stefan Leuders, Andre Riemer, Hans Albert Richard, Thomas Tröster, and Dieter Schwarze. "Highly anisotropic steel processed by selective laser melting". In: *Metallurgical and Materials Transactions B* 44.4 (2013), pp. 794–796.

[128] L. Hao, S. Dadbakhsh, O. Seaman, and M. Felstead. "Selective laser melting of a stainless steel and hydroxyapatite composite for load-bearing implant development". In: *Journal of Materials Processing Technology* 209.17 (2009), pp. 5793–5801.

[129] M. Badrossamay and T. H. C. Childs. "Further studies in selective laser melting of stainless and tool steel powders". In: *International Journal of Machine Tools and Manufacture* 47.5 (2007), pp. 779–784.

[130] Z. H. Liu, C. K. Chua, K. F. Leong, K. Kempen, L. Thijs, E. Yasa, J. Van-Humbeeck, and J.-P. Kruth. "A preliminary investigation on selective laser melting of M2 high speed steel". In: *5th International Conference on Advanced Research and Rapid Prototyping, Leiria, Portugal.* 2011, pp. 339–346.

[131] Z. H. Liu, D. Q. Zhang, C. K. Chua, and K. F. Leong. "Crystal structure analysis of M2 high speed steel parts produced by selective laser melting". In: *Materials Characterization* 84 (2013), pp. 72–80.

[132] H. Khalid Rafi, Deepankar Pal, Nachiket Patil, Thomas L. Starr, and Brent E. Stucker. "Microstructure and mechanical behavior of 17-4 precipitation hardenable steel processed by selective laser melting". In: *Journal of materials engineering and performance* 23.12 (2014), pp. 4421–4428.

[133] Luca Facchini, Nério Vicente, Ivan Lonardelli, Emanuele Magalini, Pierfrancesco Robotti, and Alberto Molinari. "Metastable Austenite in 17–4 Precipitation-Hardening Stainless Steel Produced by Selective Laser Melting". In: *Advanced Engineering Materials* 12.3 (2010), pp. 184–188.

[134] L. E. Murr, E. Martinez, J. Hernandez, S. Collins, K. N. Amato, S. M. Gaytan, and P. W. Shindo. "Microstructures and properties of 17-4 PH stainless steel fabricated by selective laser melting". In: *Journal of Materials Research and Technology* 1.3 (2012), pp. 167–177.

[135] M. Averyanova, E. Cicala, P. H. Bertrand, and D. Grevey. "Experimental design approach to optimize selective laser melting of martensitic 17-4 PH powder: part I–single laser tracks and first layer". In: *Rapid Prototyping Journal* 18.1 (2012), pp. 28–37.

[136] A. Yadollahi, N. Shamsaei, S. M. Thompson, A. Elwany, and L. Bian. "Effects of building orientation and heat treatment on fatigue behavior of selective laser melted 17-4 PH stainless steel". In: *International Journal of Fatigue* 94 (2017), pp. 218–235.

[137] Ming-Wei Wu, Pang-Hsin Lai, and Jhewn-Kuang Chen. "Anisotropy in the impact toughness of selective laser melted Ti–6Al–4V alloy". In: *Materials Science and Engineering: A* 650 (2016), pp. 295–299.

[138] W. Xu, S. Sun, J. Elambasseril, Q. Liu, M. Brandt, and M. Qian. "Ti-6Al-4V additively manufactured by selective laser melting with superior mechanical properties". In: *JOM* 67.3 (2015), pp. 668–673.

[139]   L. E. Murr, S. A. Quinones, S. M. Gaytan, M. I. Lopez, A. Rodela, E. Y. Martinez, D. H. Hernandez, E. Martinez, F. Medina, and R. B. Wicker. "Microstructure and mechanical behavior of Ti–6Al–4V produced by rapid-layer manufacturing, for biomedical applications". In: *Journal of the mechanical behavior of biomedical materials* 2.1 (2009), pp. 20–32.

[140]   P. Edwards and M. Ramulu. "Fatigue performance evaluation of selective laser melted Ti–6Al–4V". In: *Materials Science and Engineering: A* 598 (2014), pp. 327–337.

[141]   Haijun Gong, Khalid Rafi, Hengfeng Gu, Thomas Starr, and Brent Stucker. "Analysis of defect generation in Ti–6Al–4V parts made using powder bed fusion additive manufacturing processes". In: *Additive Manufacturing* 1 (2014), pp. 87–98.

[142]   Marco Simonelli, Yau Yau Tse, and Christopher Tuck. "Effect of the build orientation on the mechanical properties and fracture modes of SLM Ti–6Al–4V". In: *Materials Science and Engineering: A* 616 (2014), pp. 1–11.

[143]   Marco Simonelli, Yau Yau Tse, and Chris Tuck. "On the texture formation of selective laser melted Ti-6Al-4V". In: *Metallurgical and Materials Transactions A* 45.6 (2014), pp. 2863–2872.

[144]   Luca Facchini, Emanuele Magalini, Pierfrancesco Robotti, Alberto Molinari, Simon Höges, and Konrad Wissenbach. "Ductility of a Ti-6Al-4V alloy produced by selective laser melting of prealloyed powders". In: *Rapid Prototyping Journal* 16.6 (2010), pp. 450–459.

[145]   E. C. Santos, K. Osakada, M. Shiomi, Y. Kitamura, and F. Abe. "Microstructure and mechanical properties of pure titanium models fabricated by selective laser melting". In: *Proceedings of the institution of mechanical engineers, part c: journal of mechanical engineering science* 218.7 (2004), pp. 711–719.

[146]   D. K. Pattanayak, A. Fukuda, T. Matsushita, M. Takemoto, S. Fujibayashi, K. Sasaki, N. Nishida, T. Nakamura, and T. Kokubo. "Bioactive Ti metal analogous to human cancellous bone: fabrication by selective laser melting and chemical treatments". In: *Acta Biomaterialia* 7.3 (2011), pp. 1398–1406.

[147]   Dongdong Gu, Yves-Christian Hagedorn, Wilhelm Meiners, Guangbin Meng, Rui João Santos Batista, Konrad Wissenbach, and Reinhart Poprawe. "Densification behavior, microstructure evolution, and wear performance of selective laser melting processed commercially pure titanium". In: *Acta Materialia* 60.9 (2012), pp. 3849–3860.

[148]   Hooyar Attar, Mariana Calin, LC Zhang, Sergio Scudino, and Jürgen Eckert. "Manufacture by selective laser melting and mechanical behavior of commercially pure titanium". In: *Materials Science and Engineering: A* 593 (2014), pp. 170–177.

[149]   Tim Sercombe, Noel Jones, Rob Day, and Alan Kop. "Heat treatment of Ti-6Al-7Nb components produced by selective laser melting". In: *Rapid Prototyping Journal* 14.5 (2008), pp. 300–304.

[150] Edward Chlebus, Bogumiła Kuźnicka, Tomasz Kurzynowski, and Bogdan Dybała. "Microstructure and mechanical behaviour of Ti 6Al 7Nb alloy produced by selective laser melting". In: *Materials Characterization* 62.5 (2011), pp. 488–495.

[151] Karolien Kempen, Lore Thijs, Jan Van Humbeeck, and Jean-Pierre Kruth. "Mechanical properties of AlSi10Mg produced by selective laser melting". In: *Physics Procedia* 39 (2012), pp. 439–446.

[152] Lore Thijs, Karolien Kempen, Jean-Pierre Kruth, and Jan Van Humbeeck. "Fine-structured aluminium products with controllable texture by selective laser melting of pre-alloyed AlSi10Mg powder". In: *Acta Materialia* 61.5 (2013), pp. 1809–1819.

[153] Erhard Brandl, Ulrike Heckenberger, Vitus Holzinger, and Damien Buchbinder. "Additive manufactured AlSi10Mg samples using Selective Laser Melting (SLM): Microstructure, high cycle fatigue, and fracture behavior". In: *Materials & Design* 34 (2012), pp. 159–169.

[154] Noriko Read, Wei Wang, Khamis Essa, and Moataz M. Attallah. "Selective laser melting of AlSi10Mg alloy: Process optimisation and mechanical properties development". In: *Materials & Design (1980-2015)* 65 (2015), pp. 417–424.

[155] Christian Weingarten, Damien Buchbinder, Norbert Pirch, Wilhelm Meiners, Konrad Wissenbach, and Reinhart Poprawe. "Formation and reduction of hydrogen porosity during selective laser melting of AlSi10Mg". In: *Journal of Materials Processing Technology* 221 (2015), pp. 112–120.

[156] Karolien Kempen, Lore Thijs, Jan Van Humbeeck, and Jean-Pierre Kruth. "Processing AlSi10Mg by selective laser melting: parameter optimisation and material characterisation". In: *Materials Science and Technology* 31.8 (2015), pp. 917–923.

[157] Wei Li, Shuai Li, Jie Liu, Ang Zhang, Yan Zhou, Qingsong Wei, Chunze Yan, and Yusheng Shi. "Effect of heat treatment on AlSi10Mg alloy fabricated by selective laser melting: Microstructure evolution, mechanical properties and fracture mechanism". In: *Materials Science and Engineering: A* 663 (2016), pp. 116–125.

[158] X. J. Wang, L. C. Zhang, M. H. Fang, and Timothy B. Sercombe. "The effect of atmosphere on the structure and properties of a selective laser melted Al–12Si alloy". In: *Materials Science and Engineering: A* 597 (2014), pp. 370–375.

[159] X. P. Li, X. J. Wang, Ma. Saunders, A. Suvorova, L. C. Zhang, Y. J. Liu, M. H. Fang, Z. H. Huang, and T. B. Sercombe. "A selective laser melting and solution heat treatment refined Al–12Si alloy with a controllable ultrafine eutectic microstructure and 25% tensile ductility". In: *Acta Materialia* 95 (2015), pp. 74–82.

[160]   Johannes Strößner, Michael Terock, and Uwe Glatzel. "Mechanical and Microstructural Investigation of Nickel-Based Superalloy IN718 Manufactured by Selective Laser Melting (SLM)". In: *Advanced Engineering Materials* 17.8 (2015), pp. 1099–1105.

[161]   Qingbo Jia and Dongdong Gu. "Selective laser melting additive manufacturing of Inconel 718 superalloy parts: Densification, microstructure and properties". In: *Journal of Alloys and Compounds* 585 (2014), pp. 713–721.

[162]   A. A. Popovich, V. S. Sufiiarov, I. A. Polozov, and E. V. Borisov. "Microstructure and mechanical properties of Inconel 718 produced by SLM and subsequent heat treatment." In: *Key Engineering Materials* (2015).

[163]   Dongyun Zhang, Wen Niu, Xuanyang Cao, and Zhen Liu. "Effect of standard heat treatment on the microstructure and mechanical properties of selective laser melting manufactured Inconel 718 superalloy". In: *Materials Science and Engineering: A* 644 (2015), pp. 32–40.

[164]   Tanja Trosch, Johannes Strößner, Rainer Völkl, and Uwe Glatzel. "Microstructure and mechanical properties of selective laser melted Inconel 718 compared to forging and casting". In: *Materials letters* 164 (2016), pp. 428–431.

[165]   M. Pröbstle, S. Neumeier, J. Hopfenmüller, L. P. Freund, T. Niendorf, D. Schwarze, and M. Göken. "Superior creep strength of a nickel-based superalloy produced by selective laser melting". In: *Materials Science and Engineering: A* 674 (2016), pp. 299–307.

[166]   E. Chlebus, K. Gruber, B. Kuźnicka, J. Kurzac, and T. Kurzynowski. "Effect of heat treatment on the microstructure and mechanical properties of Inconel 718 processed by selective laser melting". In: *Materials Science and Engineering: A* 639 (2015), pp. 647–655.

[167]   M. E. Aydinöz, F. Brenne, M. Schaper, C. Schaak, W. Tillmann, J. Nellesen, and T. Niendorf. "On the microstructural and mechanical properties of post-treated additively manufactured Inconel 718 superalloy under quasi-static and cyclic loading". In: *Materials Science and Engineering: A* 669 (2016), pp. 246–258.

[168]   Md Ashabul Anam, Deepankar Pal, and Brent Stucker. "Modeling and experimental validation of nickel-based super alloy (Inconel 625) made using selective laser melting". In: *Solid Freeform Fabrication (SFF) Symposium, University of Texas at Austin, Austin, TX, Aug.* 2013, pp. 12–14.

[169]   David B. Witkin, Paul Adams, and Thomas Albright. "Microstructural evolution and mechanical behavior of nickel-based superalloy 625 made by selective laser melting". In: *SPIE LASE*. International Society for Optics and Photonics. 2015, 93530B–93530B.

[170]   Kamran Aamir Mumtaz, Poonjolai Erasenthiran, and Neil Hopkinson. "High density selective laser melting of Waspaloy®". In: *Journal of materials processing technology* 195.1 (2008), pp. 77–87.

[171] Thomas Etter, Karsten Kunze, Fabian Geiger, and Hossein Meidani. "Reduction in mechanical anisotropy through high temperature heat treatment of Hastelloy X processed by Selective Laser Melting (SLM)". In: *IOP Conference Series: Materials Science and Engineering*. Vol. 82. 1. IOP Publishing. 2015, p. 012097.

[172] Håkan Brodin, Olov Andersson, and Sten Johansson. "Mechanical behaviour and microstructure correlation in a selective laser melted superalloy". In: *ASME Turbo Expo 2013: Turbine Technical Conference and Exposition*. American Society of Mechanical Engineers. 2013, V05AT21A009–V05AT21A009.

[173] Fude Wang. "Mechanical property study on rapid additive layer manufacture Hastelloy® X alloy by selective laser melting technology". In: *The International Journal of Advanced Manufacturing Technology* 58.5 (2012), pp. 545–551.

[174] N. J. Harrison, I. Todd, and K. Mumtaz. "Reduction of micro-cracking in nickel superalloys processed by selective laser melting: a fundamental alloy design approach". In: *Acta Materialia* 94 (2015), pp. 59–68.

[175] P. Kanagarajah, F. Brenne, T. Niendorf, and H. J. Maier. "Inconel 939 processed by selective laser melting: Effect of microstructure and temperature on the mechanical properties under static and cyclic loading". In: *Materials Science and Engineering: A* 588 (2013), pp. 188–195.

[176] Guijun Bi, Chen-Nan Sun, Hui-chi Chen, Fern Lan Ng, and Cho Cho Khin Ma. "Microstructure and tensile properties of superalloy IN100 fabricated by micro-laser aided additive manufacturing". In: *Materials & Design* 60 (2014), pp. 401–408.

[177] L. Rickenbacher, T. Etter, S. Hövel, and K. Wegener. "High temperature material properties of IN738LC processed by selective laser melting (SLM) technology". In: *Rapid Prototyping Journal* 19.4 (2013), pp. 282–290.

[178] Karsten Kunze, Thomas Etter, Jürgen Grässlin, and Valery Shklover. "Texture, anisotropy in microstructure and mechanical properties of IN738LC alloy processed by selective laser melting (SLM)". In: *Materials Science and Engineering: A* 620 (2015), pp. 213–222.

[179] Fabian Geiger, Karsten Kunze, and Thomas Etter. "Tailoring the texture of IN738LC processed by selective laser melting (SLM) by specific scanning strategies". In: *Materials Science and Engineering: A* 661 (2016), pp. 240–246.

[180] M. Cloots, P. J. Uggowitzer, and K. Wegener. "Investigations on the microstructure and crack formation of IN738LC samples processed by selective laser melting using Gaussian and doughnut profiles". In: *Materials & Design* 89 (2016), pp. 770–784.

[181] Roman Engeli, Thomas Etter, Simone Hoevel, and Konrad Wegener. "Processability of different IN738LC powder batches by selective laser melting". In: *Journal of Materials Processing Technology* 229 (2016), pp. 484–491.

[182]   V. D. Divya, R. Muñoz-Moreno, O. M. D. M. Messé, J. S. Barnard, S. Baker, T. Illston, and H. J. Stone. "Microstructure of selective laser melted CM247LC nickel-based superalloy and its evolution through heat treatment". In: *Materials Characterization* 114 (2016), pp. 62–74.

[183]   R. Muñoz-Moreno, V. D. Divya, S. L. Driver, O. M. D. M. Messé, T. Illston, S. Baker, M. A. Carpenter, and H. J. Stone. "Effect of heat treatment on the microstructure, texture and elastic anisotropy of the nickel-based superalloy CM247LC processed by selective laser melting". In: *Materials Science and Engineering: A* 674 (2016), pp. 529–539.

[184]   Xiqian Wang, Luke N. Carter, Bo Pang, Moataz M. Attallah, and Michael H. Loretto. "Microstructure and yield strength of SLM-fabricated CM247LC Ni-Superalloy". In: *Acta Materialia* 128 (2017), pp. 87–95.

[185]   Maria L. Montero Sistiaga, Raya Mertens, Bey Vrancken, Xiebin Wang, Brecht Van Hooreweder, Jean-Pierre Kruth, and Jan Van Humbeeck. "Changing the alloy composition of Al7075 for better processability by selective laser melting". In: *Journal of Materials Processing Technology* 238 (2016), pp. 437–445.

[186]   M. M. Kirka, F. Medina, R. R. Dehoff, and A. Okello. "Mechanical behavior of post-processed Inconel 718 manufactured through the electron beam melting process". In: *Materials Science and Engineering: A* 680 (2017), pp. 338–346.

[187]   Kinga A. Unocic, Lindsay M. Kolbus, Ryan R. Dehoff, Sebastien N. Dryepondt, and Bruce A. Pint. "High-temperature performance of N07718 processed by additive manufacturing". In: *NACE Corrosion* 2014 (2014).

[188]   William J. Sames, Kinga A. Unocic, Grant W. Helmreich, Michael M. Kirka, Frank Medina, Ryan R. Dehoff, and Sudarsanam S. Babu. "Feasibility of in situ controlled heat treatment (ISHT) of Inconel 718 during electron beam melting additive manufacturing". In: *Additive Manufacturing* 13 (2017), pp. 156–165.

[189]   R. R. Dehoff, M. M. Kirka, F. A. List, K. A. Unocic, and W. J. Sames. "Crystallographic texture engineering through novel melt strategies via electron beam melting: Inconel 718". In: *Materials Science and Technology* 31.8 (2015), pp. 939–944.

[190]   Narendran Raghavan, Ryan Dehoff, Sreekanth Pannala, Srdjan Simunovic, Michael Kirka, John Turner, Neil Carlson, and Sudarsanam S. Babu. "Numerical modeling of heat-transfer and the influence of process parameters on tailoring the grain morphology of IN718 in electron beam additive manufacturing". In: *Acta Materialia* 112 (2016), pp. 303–314.

[191]   K. N. Amato, S. M. Gaytan, L. E. Murr, E. Martinez, P. W. Shindo, J. Hernandez, S. Collins, and F. Medina. "Microstructures and mechanical behavior of Inconel 718 fabricated by selective laser melting". In: *Acta Materialia* 60.5 (2012), pp. 2229–2239.

[192] Joon-Phil Choi, Gi-Hun Shin, Sangsun Yang, Dong-Yeol Yang, Jai-Sung Lee, Mathieu Brochu, and Ji-Hun Yu. "Densification and microstructural investigation of Inconel 718 parts fabricated by selective laser melting". In: *Powder Technology* 310 (2017), pp. 60–66.

[193] Zemin Wang, Kai Guan, Ming Gao, Xiangyou Li, Xiaofeng Chen, and Xiaoyan Zeng. "The microstructure and mechanical properties of deposited-IN718 by selective laser melting". In: *Journal of Alloys and Compounds* 513 (2012), pp. 518–523.

[194] Derek H. Smith, Jonathan Bicknell, Luke Jorgensen, Brian M. Patterson, Nikolaus L. Cordes, Igor Tsukrov, and Marko Knezevic. "Microstructure and mechanical behavior of direct metal laser sintered Inconel alloy 718". In: *Materials Characterization* 113 (2016), pp. 1–9.

[195] Yen-Ling Kuo, Shota Horikawa, and Koji Kakehi. "The effect of interdendritic δ phase on the mechanical properties of Alloy 718 built up by additive manufacturing". In: *Materials & Design* 116 (2017), pp. 411–418.

[196] Xiaoqing Wang and Kevin Chou. "Electron Backscatter Diffraction Analysis of Inconel 718 Parts Fabricated by Selective Laser Melting Additive Manufacturing". In: *JOM* (2016), pp. 1–7.

[197] Paul S Prevéy. "A method of determining the elastic properties of alloys in selected crystallographic directions for X-ray diffraction residual stress measurement". In: *Advances in X-ray Analysis* 20 (1977), pp. 345–354.

Part Part II:

Included papers

知不知上，不知知病。
夫唯病病，是以不病。
聖人不病，以其病病，是以不病。
《道德經》

Papers

The papers associated with this thesis have been removed for copyright reasons. For more details about these see:

尴尬亦切记淡定！